Construction and Building Materials 385 (2023) 131223

Contents lists available at ScienceDirect

Construction and Building Materials

journal homepage: www.elsevier.com/locate/conbuildmat

Understanding the role of a novel internal conditioning technique with functionalized montmorillonite in cement hydration kinetics

Dayou Luo, Jianqiang Wei *

Department of Civil and Environmental Engineering, Francis College of Engineering, University of Massachusetts Lowell, Lowell, MA 01854, USA

ARTICLE INFO

Keywords:
Internal conditioning
Montmorillonite
Hydration kinetics
Activation energy
Phase evolution
Property development

ABSTRACT

A novel internal conditioning (InCon) technique based on saturated sodium montmorillonite (sMT) functionalized with two non-ionic surfactants, polyoxyethylene (9) nonylphenylether and *t*-octyl phenoxy poly ethoxyethanol, is investigated in this study. With the integration of water for internal curing and pozzolanic reactivity in a single system, the role of InCon in modifying cement hydration kinetics is comprehensively elucidated. The results indicate that, in the presence of InCon, both silicate reaction and secondary aluminate reaction rates are enhanced, and the apparent activation energy (*Ea*) of cement hydration was decreased from 34.3 KJ/mol to 28.7 KJ/mol indicating a lower temperature sensitivity and threshold of the cement hydration reactions. In addition, decreased CH contents, improved degree of hydration, increased chemical shrinkage, and the formation of additional C—S—H and aluminum-containing phases were obtained from the cement with InCon. The autogenous shrinkage of cement and the negative impact of dry sMT on the early age strength of cement can be offset by InCon paving a new path to improve the overall properties of concrete.

1. Introduction

Cement hydration involves a series of chemical reactions between water, clinker components (i.e., alite (C_3S), belite (C_2S), aluminate (C_3A), and ferrite (C_2(A, F) phases) and calcium sulfate, spanning multiple time and length scales. As the cement hydration proceeds, the reaction products are packed closely to form densified structures contributing to setting and hardening [1,2]. In this critical process, water availability and space accessibility for hydration products dominate the maximum attainable degree of hydration (DOH) of cement [3]. In the presence of a high water-to-cement (w/c) ratio, a high DOH can be easily reached, while more crystalline portlandite can be produced, which exhibits a preferential direction of fracture and provides space for potential crack propagation attributing to the reduction of strength. Therefore, a low w/c ratio is typically preferred to obtain high strength with a homogenous dispersion of calcium-bearing calcium silicate hydrates (C—S—H). In addition, a lower w/c ratio would result in a lower and less continuous porosity retarding the internal transport and decreasing penetration of external deleterious ions, such as chloride, sulfate, alkalis, etc. [4], thereby improving the resistance of concrete against a variety of degradation mechanisms. However, in the presence of low w/c ratios, the DOH and hydration products decrease [5]. It was reported that the internal relative humidity (RH) threshold for triggering the cement hydration reactions is at least 80 % [6], as the alite normally stops hydration at a lower RH [7]. When the w/c ratio is lower than 0.36, which is especially the cases of high strength or ultra-high performance concrete, the spare space is not enough for the continuous production growth, and extra water from an external source is required to achieve the complete cement hydration with a mediate w/c ratio value between 0.36 and 0.42 [8]. How to maximize the DOH to take full advantage of cement in concrete at a low w/c ratio to enhance strength and durability [9] and to address the challenges of shrinkage and cracking [10] in a single system has been a critical challenge that remains for many years.

Different from the conventional external curing in which insufficient water can be readily penetrated into concrete [11,12], internal curing shows promising potential to address the aforementioned challenges. The basic concept of internal curing is carrying and gradually releasing extra water triggered by distributed reservoirs in concrete with an ignorable impact on the initial w/c ratio [13]. By pre-soaking (or pre-saturating) the reservoir agents, a more even and efficient distribution of water within the matrix of concrete can be achieved, which makes the

* Corresponding author at: Department of Civil and Environmental Engineering, University of Massachusetts Lowell, 1 University Avenue, Shah Hall 200, Lowell, MA 01854, United States.
E-mail address: jianqiang_wei@uml.edu (J. Wei).

https://doi.org/10.1016/j.conbuildmat.2023.131223
Received 12 September 2022; Received in revised form 11 March 2023; Accepted 27 March 2023
Available online 28 April 2023

Table 1
Chemical and mineralogical compositions of the cementing materials.

Comp.	CaO	SiO_2	Al_2O_3	SO_3	Fe_2O_3	MgO	SrO	K_2O	Na_2O	TiO_2	ZnO	Cl	Compton	Rayleigh
sMT	0.95	62.0	17.2	0.20	6.52	7.35	0.04	0.072	5.03	0.23	0.03	0.19	0.86	1.03
Cement	62.7	20.1	4.8	3.5	3.2	3.4	Equivalent alkali			C_3S	C_2S	C_3A	C_4AF	LS
							0.6			54	17	7	10	1.2

Note: Equivalent alkali: $Na_2O + 0.658K_2O$; C_3S: tricalcium silicate; C_2S: dicalcium silicate; C_3A: tricalcium aluminate; C_4AF: tetra-calcium aluminoferrite; LS: limestone; $CaCO_3$ in LS: 92.0 %.

curing efficiency outperform conventional external curing. A variety of materials, such as lightweight aggregates (LWA) [14], crushed returned concrete fines [15], superabsorbent polymers [16], fly ash cenospheres [17], zeolite [18], rice husk ash[19], and wood pulp fibers [20], have been investigated as reservoirs in internally cured concrete. However, side effects of conventional internal curing have been reported. The highly porous structure and poor mechanical properties of the nonreactive or low reactive agents were found to detrimentally impact the strength [21], durability [22], and elastic modulus [23] of concrete.

Montmorillonite (MT) is the primary component of naturally abundant sludges and bentonite with a 2:1 sandwiched layered structure consisting of two stacked tetrahedral silicate sheets and an octahedral aluminate sheet in-between. As a representative of supplementary cementitious materials (SCMs), MT is rich in amorphous aluminate and silicate with a high specific surface area [24,25] thereby possessing high pozzolanic reactivity, but it typically shows intermediate reactivity compared to kaolinite after either thermal [26] or mechanochemical activation [27]. The pozzolanic reaction between MT and calcium hydroxide (CH) produced by cement hydration leads to the formation of additional C—S—H or aluminum-bearing C—S—H (C-A—S—H), which is mostly responsible for the strength gain of concretes [13,28]. As a result, enhanced cement hydration, densified microstructure, lower permeability, higher mechanical strength, and increased durability of concrete could be obtained by partially substituting cement with MT [29–31]. However, the poor dispersion of MT nanoparticles in the cement matrix due to their high agglomeration in the ionic environment was identified as the main issue impeding its bulk substitution in the cement industry with a limited optimal substitution level (1 %-3% by mass) [32]. Both the pozzolanic reactivity of the MT and the performance of concrete would be negatively impacted at higher substitution levels [26,30]. Recently, the exchangeable cations (i.e., sodium, potassium, calcium, and magnesium) in the interlayer spaces of MT that can counterbalance the negative charge caused by the partial replacement of Si^{4+} by Al^{3+} in tetrahedral sheets [33] were exploited to fabricate desirable surfactant functionalized MT with better dispersion and higher pozzolanic reactivity in the cement matrixes [34–36]. In the authors' previous study, functionalization and property characterization of sodium MT (sMT) were investigated and the potential of the functionalized sMT as an agent for internal curing of concrete has been experimentally explored. Although the improved dispersion, pozzolanic reactivity, as well as the unique water uptake capacity (WUC) and release behavior of the functionalized sMT [37] are promising, its role in enhancing cement hydration has not been elucidated.

In light of the promising properties of the functionalized sMT, the present study aims to develop a novel internal conditioning (InCon) technique to combine the benefits of internal curing and pozzolanicity in a single system based on functionalized sMT by two non-ionic surfactants, i.e., polyoxyethylene (9) nonylphenylether (PONPE9) and *t*-octyl phenoxy poly ethoxyethanol (TX100). The kinetics and apparent activation energy (E_a) of the hydration of cement composites containing the functionalized sMT-based InCon were explored based on the heat of hydration via isothermal calorimetry at varying temperatures coupling with the Arrhenius theory. To obtain a comprehensive understanding of phase evolution in the internally conditioned cement systems, the hydration products were characterized and quantified using thermogravimetric analysis (TGA), X-ray diffraction analysis (XRD), attenuated total reflectance-Fourier transform infrared (ATR-FTIR), Raman spectroscopy, as well as microstructure analysis via field emission scanning electron microscopy (FE-SEM). Property development of the cement composites including chemical shrinkage, autogenous shrinkage, and compressive strength were also monitored. The results of this study are expected to provide elucidation on the influence of the novel InCon on the hydration behavior of cement and pave a path for its applications in high-performance concrete.

2. Materials and methods

2.1. Materials

Type I/II ordinary Portland cement (ASTM C150 [38]) produced by Quikrete and fine sMT powders (Sigma-Aldrich) were used as the cementitious raw materials in this study. Table 1 shows the chemical

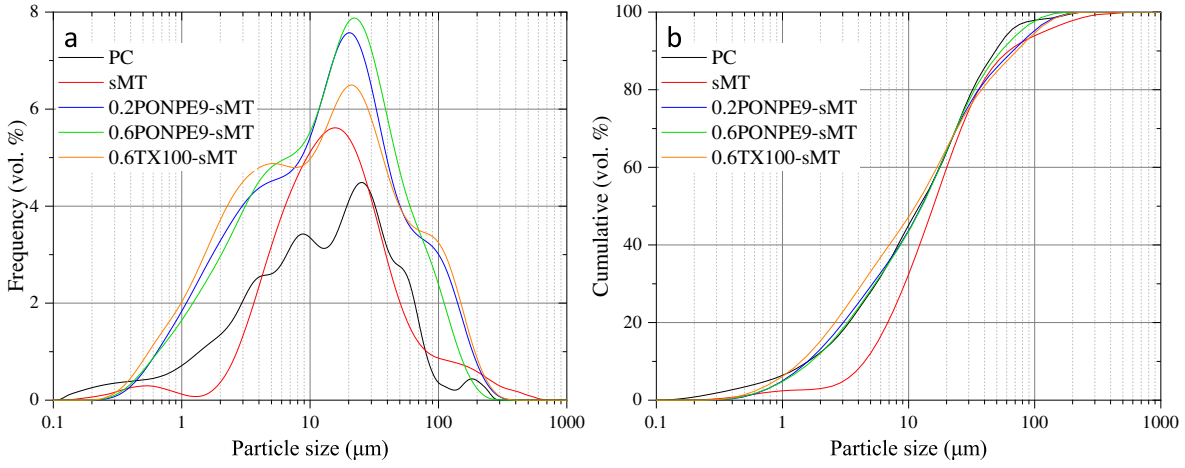

Fig. 1. Particle size distributions of the cement, raw and functionalized sMTs: (a) relative frequency and (b) volume of the particles smaller than a specific diameter.

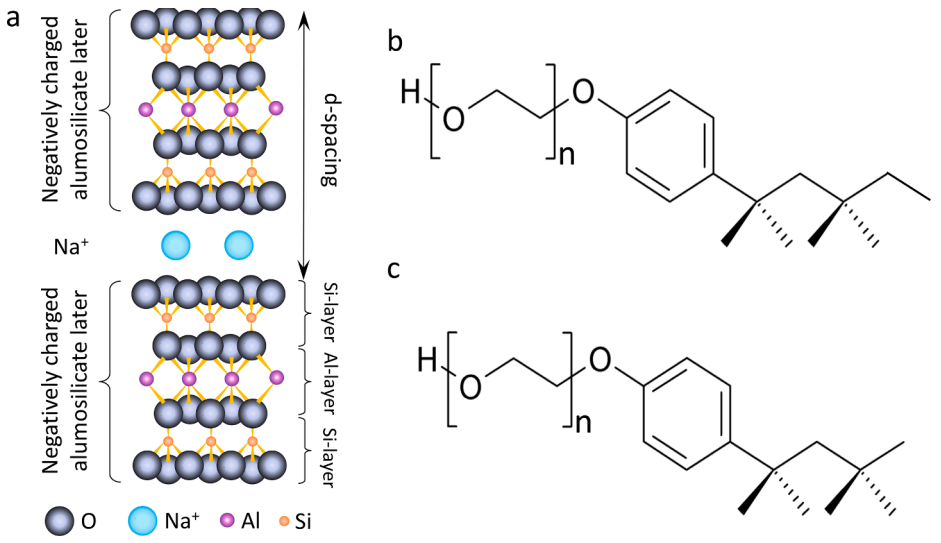

Fig. 2. Chemical structures of (a) sMT, (b) PONPE9 and (c) TX100.

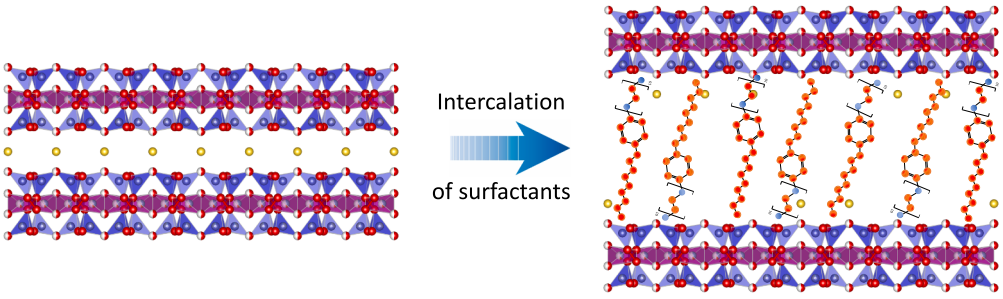

Fig. 3. Schematic diagram for the structure change of sMT due to the intercalation of the surfactants.

compositions of the cement and sMT, where it can be seen that the silicate and aluminate phases (SiO_2 + Al_2O_3) occupy>79 wt% in sMT. Fig. 1 presents particle size distributions (PSD) of cement and sMT measured by laser diffraction. The cement and sMT possess median particle sizes of 12.2 μm and 15.7 μm, respectively. According to the manufacturer, the relative density and molecular weight of the sMT are 2.4 g/cm^3 and 180.1 g/mol, respectively. Based on the Methylene blue test per ASTM C837 [39], the cation exchange capacity (CEC) of sMT was determined as 116.48 meq/100 g. In this study, the as-received sMT was organically functionalized by two chemically pure non-ionic surfactants, PONPE9 and TX100 (Sigma-Aldrich), with an average molar mass of 660 g/mol and 647 g/mol, respectively. Fig. 2a, 2b, and 2c present the schematic molecular structures of sMT and the two non-ionic surfactants.

The ion-exchange method [40], which is controlled by nanoscale chemical–mechanical coupling [41], was employed to organically functionalize sMT by mixing sMT particles with PONPE9 or TX100 in deionized (DI) water at 25 ℃. 100 g of sMT, and the specific amount of surfactant (either PONPE9 or TX100) at 0.2 CEC or 0.6 CEC were magnetically stirred in 1 L DI water at 500 rpm for 30 min, followed by

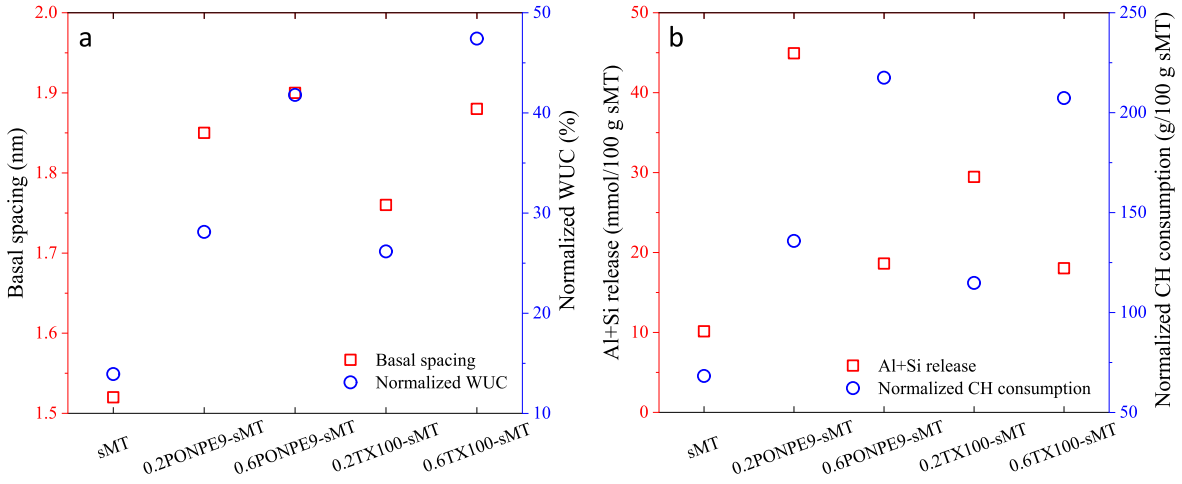

Fig. 4. (a) Basal spacing and normalized water uptake capacity; (b) released "Al + Si" and normalized CH consumption of the raw and functionalized sMTs.

Table 2
Compositions of cement mixtures.

Index	Content (g) Cement	sMT	Mixing Water	InCon water	Sand	w/b
PC	100	0	40	0	100	0.40
DsMT	97	3	40	0	100	0.40
SsMT	97	3	40	0.417	100	0.40
0.2PONPE9-SsMT	97	3	40	0.842	100	0.40
0.6PONPE9-SsMT	97	3	40	1.251	100	0.40
0.2TX100-SsMT	97	3	40	0.784	100	0.40
0.6TX100-SsMT	97	3	40	1.422	100	0.40

centrifugation at 1400 rpm for 15 min to separate the functionalized sMTs from the suspension. After a 24-h oven drying at 70 °C, the functionalized sMTs were grounded with a planetary ball mill at 900 rpm for 2 h, followed by a sieving process to obtain ultra-fine particles smaller than 40 μm. As shown in Fig. 1, after ball milling, the median particle sizes of the finctionalized sMTs are within a range of 11.3–12.8 μm, which is slightly lower than that of the raw sMT. More details of the functionalization process can be found in the author's previous work [37]. A schematic diagram of the layered sMT clay structures before and after the functionalization is presented in Fig. 3. The concentrations of the surfactants employed in this study are equivalent to 0.2 or 0.6 CEC of sMT, and the functionalized clay was expressed as "*xy*-sMT", where *x* is the equivalent loading of the surfactants with respect to the CEC and *y* is the names of the surfactants. For example, 0.2PONPE9-sMT means the sMT functionalized by PONPE9 at a dosage of 15.38 g/100 g sMT, which is equivalent to 0.2 CEC of the raw sMT.

Fig. 4 summarizes the properties of sMT before and after the functionalization with the two surfactants. As shown in Fig. 4a, after functionalization, the basal spacing of sMT was increased from 1.52 nm up to 1.90 nm, varying with different surfactants and dosages. Herein, significant improvements in WUC of sMT from 13.92 % to 47.42 % (0.6TX100-sMT) were also obtained. As a result, the pozzolanic reactivity of sMT was also improved after functionalization. As shown in Fig. 4b, the Al + Si dissolved from the clay particles into a simulated concrete pore solution was increased from 10.13 mmol/100 g sMT to a maximum value of 44.93 mmol/100 g sMT. As a result, the CH consumption capacity was raised from 68.21 g/100 g sMT to 217.5 g/100 g sMT (0.6PONPE9-sMT). A more comprehensive insight and discussion can be found in the authors' previous study [37].

2.2. Sample preparation

The mix design for the cement blends is summarized in Table 2. In this study, 7 groups in total, including neat Portland cement (PC) as a control group, a cement-dry sMT blend (DsMT), a cement-saturated sMT blend (SsMT), and four cement blends containing saturated sMT functionalized by PEG-10 and TX-100 at 0.2 and 0.6 CEC (0.2PONPE9-SsMT, 0.6PONPE9-SsMT, 0.2TX100-SsMT, 0.2TX100-SsMT), were prepared. The water-to-binder (w/b) ratio and cement replacement level were fixed at 0.40 and 3 wt%, respectively. The weight of the surfactants was taken into account to ensure that all the binary cement blends have the same amount of sMT (see Table 2). The saturated raw and functionalized sMTs were prepared according to their WUC as shown in Fig. 4a.

The cement and cement-sMT pastes were mixed in a vacuum mixer at 500 rpm for 3 min to obtain homogenous mixtures and avoid air bubbles, and then sealed in plastic containers at 23 ± 2 °C. At each testing age for TGA, XRD, ATR-FTIR, and Raman spectroscopy analysis, the paste samples were ground into fine powders, and then the cement hydration was stopped by solvent exchanging with alcohol for 24 h. After 90 days, SEM analysis was conducted on thin disks cut from the hydrated samples. Mortar samples based on the same proportioning shown in Table 2 with a binder-to-sand ratio of 1.0 were prepared for compressive strength evolutions. The cement pastes were mixed with gradually added sand in a mechanical mortar mixer at 60 rpm for 2 min, followed by a 1-minute rest, and another 3 min of faster mixing at 120 rpm. Then, three 25 mm by 25 mm by 25 mm cubic samples were cast for each group per each testing age. After 24 h of covering with a plastic sheet, the specimens were demolded and cured in saturated CH solution at 23 ± 2 °C until testing.

2.3. Experimental methods

2.3.1. Isothermal calorimetry

To understand the influence of InCon on the hydration kinetics of cement, the heat flow and cumulative heat release of the cement pastes during the first 50 h were measured with an I-Cal 2000 HPC high precision isothermal calorimeter at temperatures of 25 °C, 40 °C, and 55 °C. Before mixing, the raw materials for each measurement, i.e., cement, raw or the functionalized sMTs (in dry or pre-saturated condition) and mixing water, were conditioned in the calorimeter chambers at the target temperatures for 24 h. After the temperature of the raw materials was stabilized, 50 g pastes with a w/b ratio of 0.40 were mixed homogeneously by hand in an oven at the same target temperatures. Immediately after being well-mixed, the paste samples were sealed in plastic containers and placed in the calorimeter chambers for data collection. The entire mixing and sample placing process was completed within 1 min to minimize the potential influence on the hydration heat evolution. At the elevated temperatures, a slight descending trend was detected from the heat flow curves, which might be due to the water evaporation from the sealed plastic vials. It was reported that the heat loss due to water evaporation is independent of the mixture compositions and nearly the same as the case when the plastic vial was filled with pure water [42]. In this study, the measured heat evolution induced by water evaporation was considered to correct the heat evolution at elevated temperatures.

Based on the isothermal calorimetry data, a modified ASTM C1074 [43] approach was adapted to calculate E_a (KJ/mol), in which the cumulative heat release curves were fitted using the three-parameter model given in Eq. (1).

$$H(t) = H_u \bullet \exp[-(\tau/t)^{\beta}] \quad (1)$$

where $H(t)$ is the cumulative heat release at time t, and $H(u)$, τ, and β are the ultimate cumulative heat release, heat release time parameter (hours), and heat release rate constant, respectively.

Then, the Arrhenius theory was followed to plot the linear fitting of $\ln(\tau)$ versus $1/T$, see Eq. (2). E_a was calculated by multiplying the slope of the best-fit line and the R-value.

$$ln[\tau] = (E_a/R) \bullet (1/T) + lnA \quad (2)$$

where R is the natural gas constant (8.314 J/mol/K), T is temperature (K) and A is the pre-exponential factor.

2.3.2. Thermogravimetric analysis

TGA was carried out on 20–40 mg of ground powders of the paste samples after 7, 28, and 90 days using a Perkin Elmer TGA 4000 thermogravimetric analyzer from ~ 30 °C to ~ 800 °C at a heating rate of 15 °C/min under inert N_2 gas environment. The content of CH was determined from the weight loss between 400 °C and 570 °C and the CH converted from the detected calcium carbonate (CC), which is due to the carbonation of CH in the samples during processing (see Eq. (3)). The content of CC was determined based on the weight drop between ~590 °C and ~770 °C by excluding the limestone (LS) content in the cement as shown in Eq. (4). It should be noted that the temperature boundaries of CH and CC might slightly vary for specific samples, i.e.,

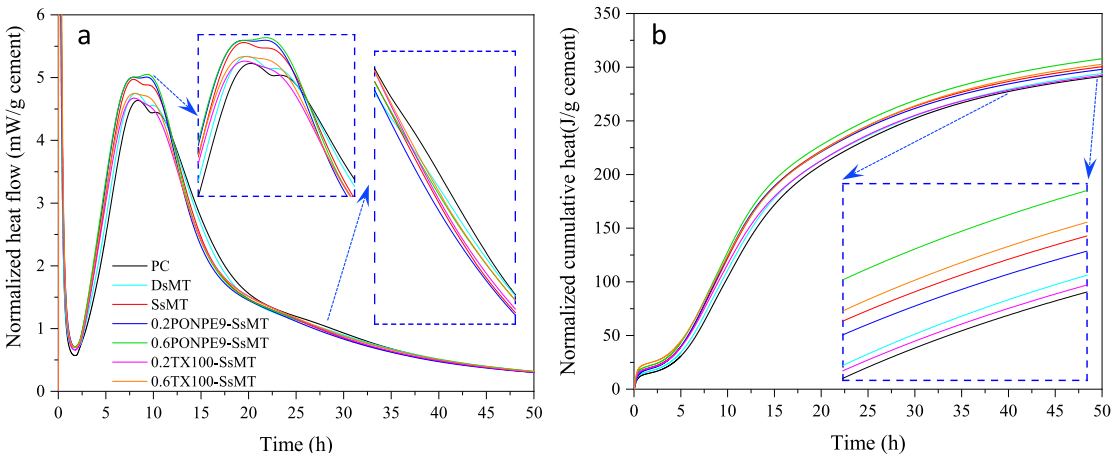

Fig. 5. (a) Normalized heat flow and (b) normalized heat release at 25 °C.

the temperatures are not fixed at the values shown in Eq. (3) and Eq. (4). Instead, a tangent method [44] was applied to determine the temperature ranges based on the TGA and differential thermogravimetric analysis (DTG) curves.

$$CH = \left[\frac{W_{400} - W_{510}}{W_{510}}\right] \bullet \left(\frac{M_{CH}}{M_{H_2O}}\right) + CC \bullet \left(\frac{M_{CH}}{M_{CC}}\right) = 0.41[(W_{400} - W_{510})/W_{510}] + 0.74CC \quad (3)$$

$$CC = [(W_{590} - W_{770})/W_{770}] \bullet (M_{CC}/M_{CO_2}) - f_C \bullet LS = 2.27[(W_{590} - W_{770})/W_{770}] - f_C \bullet LS \quad (4)$$

where W_n is the mass at temperature n °C, and M_x is the molar mass of each component (i.e., CH, H_2O, CC, and CO_2).

As shown in Eq. (5), the content of the chemically bound (non-evaporable) water (W_B) in the cement systems was determined by summing the water loss in the dihydroxylation of CH as determined in Eq. (3) and that due to the dehydration of C—S—H, ettringite (AFt), strätlingite, and calcium monosulfoaluminate (AFm) in between 120 and 400 °C.

$$W_B = Ldh + Ldx = Ldh + 0.243CH \quad (5)$$

where *Ldh* and *Ldx* represent the mass loss during the dehydration and dehydroxylation stages, respectively.

A modified Bhatty method [45] was employed to calculate the DOH of cement by normalizing W_B with the mass fraction of cement in the blends (f_c) and the ultimate chemically bound water per gram of fully hydrated cement (0.25 g/g) [46,47]:

$$DOH = W_B/(0.25 \bullet f_C) \quad (6)$$

2.3.3. X-ray diffraction analysis

XRD patterns of the ground cement paste powders after 7, 28, and 90 days of hydration were captured by an AXRD powder X-ray diffractometer equipped with a CuKα source ($\lambda = 1.54$ Å) at 30 kV and 20 mA. The scanning was performed in stepwise mode between 15° and 65° with a step size of 0.02° (2θ) and a scanning time of 5 s per step. XRDWIN®PD combined with the Crystallography Open Database (COD) [48] was used for peak fitting and phase identification. In the Rietveld refinement analysis, the background was fitted by 7th order of Chebyshev polynomial and then subtracted from the original data, followed by quantification based on the Voigt model. The unhydrated alite and belite were quantified and compared with the DOH of cement determined by TGA.

2.3.4. Chemical shrinkage

The chemical shrinkage of the cement pastes was determined by following ASTM C1608 (2017) [49], with two repetitions at a temperature of 23 ± 2 °C. The cement pastes were prepared by mixing the raw materials listed in Table 1 in a vacuum mixer at 500 rpm for 3 min to ensure homogenous mixtures with no air bubbles. About 10 g of fresh pastes were cast in a 50-mL plastic cylindrical container to reach a thickness of about 10 mm. DI water was slowly added to fill the rest of the container. Rubber stoppers equipped with graduated capillary pipets with a resolution of 0.01 mL were applied to seal the vials and the air bubbles were completely removed when assembling the rubber stoppers. One drop of paraffin oil was added to the top of the water in the graduated capillary pipets to stop the water evaporation. During the first 4 h, chemical shrinkage was recorded every 30 min, and then every 1 h up to 8 h, followed by once a day for up to 30 days.

2.3.5. ATR-FTIR and Raman spectroscopy

ATR-FTIR spectra in the range of 4000 ~ 400 cm^{-1} were collected for all the ground cement pastes after 7, 28, and 90 days using a Thermo Fisher Scientific Nicolet iS10 FTIR spectrometer by pressing the powders to the ATR diamond to interact with the IR light based on the co-addition of 32 scans with a resolution of 4 cm^{-1}.

After 7 and 90 days of hydration, Raman spectra were recorded by loading the grounded cement powders after compacting them onto a glass slide using a Horiba LabRam HR Evolution Raman spectrometer with a 532 nm excitation laser source and 2.8 mW laser power. The scanning was conducted under a 50 × objective lens in the range of 200 cm^{-1} to 1700 cm^{-1} with a resolution of 0.5 cm^{-1} and an acquisition time of 60 s with 2 accumulations. The background of the as-received data was removed using LabSpec 6 Spectroscopy Suite, and the peaks were fitted with the Gaussian function.

2.3.6. Compressive strength

ASTM C109 [50] was followed to determine the compressive strength of the mortars on a CONTROLS automatic concrete compression machine at a loading rate of 900 N/s. The strength tests were performed after 1, 7, and 90 days on the cubic mortar specimens with three repetitions, the average of which was used as the representative strength.

2.3.7. Microstructure analysis

The microstructure analysis of the hydration products of selected cement pastes after 90 days of hydration was performed on polished cutting surfaces using a JEOL JSM 7401F FE-SEM under an accelerating voltage of 10.0 kV.

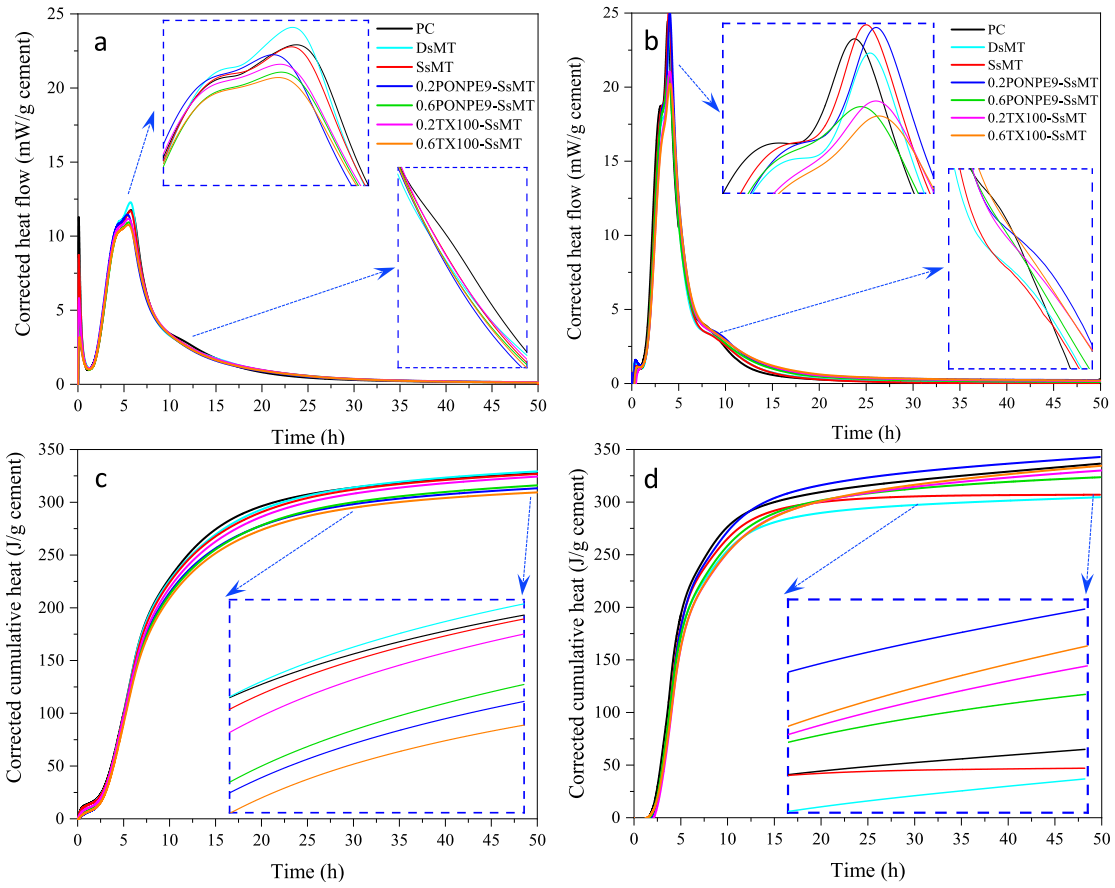

Fig. 6. Corrected heat flow at (a) 40 °C, (b) 55 °C, and corrected cumulative heat release at (c) 40 °C, (d) 55 °C.

3. Results

3.1. Isothermal calorimetry

The measured heat flow and cumulative heat release of neat PC, binary cement blends containing dry/pre-saturated raw and functionalized sMTs normalized by the mass fraction of cement at 25 °C are shown in Fig. 5a and 5b, respectively. From the heat flow curves in Fig. 5a, the five typical stages, namely the pre-induction stage due to the rapid hydration of C_3A occurring immediately after contacting with water (during the first 0.1 h), the induction stage with the minimal hydration activity, the end of which marks the onset of the main reactions (0.1 to 2.5 h), the acceleration (2.5 to 18 h) and deceleration (22 to 30 h) showing the two main peaks due to the reactions of silicate and secondary hydration of C_3A, and the diffusion-controlled steady stage (up to the end of the test) with low heat release can be identified. As defined in [51], the first main peak in the heat flow curves represents the hydration rate of alite, and the time to reach the maximum hydration rate (T_{max}) can be used to evaluate the acceleration of hydration. A broad shoulder between 25 and 30 h corresponding to the conversion of ettringite to AFm phases was also observed. By incorporating 3 wt% dry sMT, the peaks corresponding to silicate and secondary aluminate reactions occurred 0.2 and 0.3 h earlier than the neat PC group with 2.3 % and 2.4 % higher amplitudes, respectively. This indicates the accelerated and enhanced early cement hydration in the presence of sMT. The same phenomenon was also observed from the cumulative heat release curve in Fig. 5b, wherein 2.7 J/g cement more hydration heat was released after 50 h of hydration by adding the dry sMT. When the dry sMT was changed to saturated sMT, not only the amplitude of the peaks was further raised, but also the exothermic peaks were further brought forward (7.9 and 9.5 h). Around 3.1 % and 2.2 % higher heat were released from the SsMT group than in the PC and DsMT groups, respectively. These observations revealed that the saturated sMT-based InCon plays a more favorable role in enhancing and accelerating cement hydration than the traditional substitution of dry sMT. The high silica and alumina contents of the sMT might explain the increased heat flow, while the accelerated hydration was probably attributed to the finer particle size of sMT that provides more nucleation sites for C—S—H [52]. Compared with sMT, the further accelerated cement hydration from the SsMT group might be due to (1) the release of the bearing water and (2) spare spaces provided by the volume change (shrinkage) of saturated sMT after releasing water. After 20 h, the hydration heat flow of PC exceeded that of DsMT and SsMT groups, suggesting the retarded conversion of ettringite into AFm in the presence of DsMT, which becomes more significant in SsMT.

Comparing with SsMT, as shown in Fig. 5a, higher exothermic peaks were yielded by the cement pastes containing saturated PONPE9-functionalized sMTs, while no further acceleration of these peaks was observed. 0.6PONPE9-SsMT presented a comparable amplitude for the silicate reaction peak but a slightly higher peak for the secondary aluminate reaction than 0.2PONPE9-SsMT. While both of the PONPE9 functionalized sMTs resulted in higher cumulative heat releases than PC, when comparing with SsMT, 0.2PONPE9-SsMT exhibited 0.8 % lower 50-hour cumulative heat release while 0.6PONPE9-SsMT presented a 2.5 % higher value (Fig. 5b). This more pronounced cement hydration enhancement might be due to the higher pozzolanic reactivity, better dispersion, and more InCon water of the clay particles intercalated with 0.6CEC of PONPE9. The heat flow peaks of the two TX100-SsMT groups were found to be higher than that of PC but lower than SsMT. As shown in Fig. 5b, 0.2TX100-SsMT presented a slightly lower cumulative heat flow than PC, while 0.6TX100-SsMT released 0.7 % more heat than SsMT. This indicates that, at the same dosages, TX100 is less effective

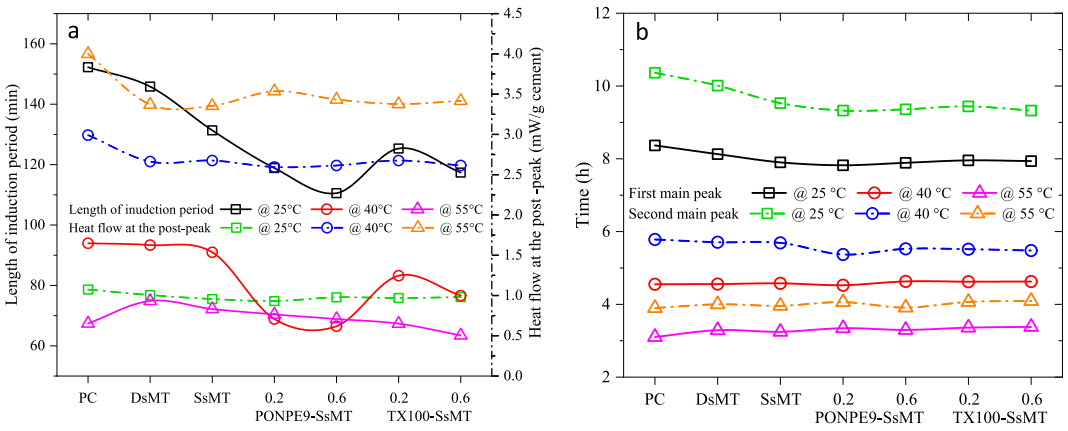

Fig. 7. (a) Changes in the length of the induction period and heat flow at the "post-peak" and (b) the time of the first and second main peaks for the cement blends at various temperatures.

than PONPE9 in improving the role of sMT in enhancing the early-age hydration of cement.

The heat flow and cumulative heat release curves at elevated temperatures of 40 °C and 55 °C were also tested, while a downtrend after around 25 h was observed from the accumulative heat release curves at 55 °C (see Fig. A1 in Appendix A). This might be due to the undesired water evaporation from the samples during the calorimetry test. The same phenomenon and issue have been identified in previous studies [42,53,54], which results in limited insights into cement hydration kinetics. It was found that, at a high temperature of 87 °C, about 0.03 g/day of water can be evaporated resulting in about 0.02 mW/day of heat loss [42]. Although this minor heat loss has an insignificant impact on the heat flow data, it can induce a non-negligible change in the cumulative heat release curves, especially in the later ages when the hydration heat from cement is reaching equilibrium, which results in underestimated long-term hydration heat.

To address this issue, the heat loss caused by water evaporation under the same elevated temperatures was tested, which was then taken into account to correct the heat flow and release evolutions. Fig. 6 presents the corrected heat flow and heat release curves at temperatures of 40 °C and 50 °C. It can be seen that the heat evolution was significantly accelerated and increased by the curing temperature. Firstly, compared with that at 25 °C, the pre-induction and induction periods both decreased with the higher temperatures. The induction period ends at around 1.2 and 0.9 h at 40 °C and 55 °C, respectively, which were 1.3 and 1.6 h earlier than that at 25 °C. Secondly, the acceleration and deceleration stages occurred earlier and the exothermic peaks became narrower and shaper with higher amplitudes. The maximal exothermic peak caused by the reaction of silicate was accelerated from 9.5 h to 5.8 and 3.8 h when the curing temperature was raised from 25 °C to 40 and 55 °C, respectively. Moreover, different from the case at 25 °C, the silicate reaction peak in the functionalized sMT groups is lower than that in the PC, while SsMT and 0.2PONPE9-SsMT exhibited a higher peak than PC. The broad shoulder due to the conversion of AFt to AFm was also accelerated under the elevated temperatures, while PC still presented the highest amplitude (Fig. 6a), which is the same as the phenomenon observed at 25 °C. At 55 °C, further enhanced cement hydration was observed from all the groups, while the differences between the groups became less significant indicating that the cement hydration is less sensitive to the additives at a high temperature. As a result of the enhanced cement hydration, higher cumulative heat release increasing with the raised temperature was observed (Fig. 6c and 6d). PC yielded 50-h heat release of 327.5 and 336.5 J/g cement at 40 °C and 55 °C, respectively, which were 12.4 % and 15.5 % higher than that at 25 °C. Interestingly, different from the detected data at 25 °C, only 0.2PONPE9-SsMT showed 1.8 % higher cumulative heat release than PC at 55 °C, while the groups containing other functionalized SsMTs exhibited lower values than PC at higher temperatures (see Fig. 6c and 6d), indicating the decreased temperature sensitivity.

According to the graphic method proposed by [55], the length of the induction period could be determined from the normalized heat release curves by the intersections of a horizontal baseline at the lowest point with the tangent lines of the decrease stage in the pre-induction peak and that of the increase stage in the acceleration period. It can be seen from Fig. 7a that the induction period of cement hydration was shortened in the presence of the raw and functionalized sMTs at 25 °C and 40 °C. The PC presented an induction period of 152.3 min at 25 °C and it decreased to 90.3 min and 65.9 min at 40 °C and 55 °C, respectively. By incorporating 3 % dry sMT, the induction period decreased by 6.5 min and 0.6 min at 25 °C and 40 °C, respectively, while it extended by 6.8 min at 55 °C. The same trend was also observed from SsMT, 0.2PONPE9-SsMT, and 0.6PONPE9-SsMT. Moreover, at each temperature, the length of the induction period follows the order of PC > DsMT > SsMT > 0.2PONPE9-SsMT > 0.6PONPE9-SsMT. TX100-SsMT groups exhibited a shorter induction period than PC, DsMT, and SsMT, while a higher dosage of TX-100 in sMT further decreased the induction period, which is in line with PONPE9. Interestingly, less diversity was found among the groups at the higher temperatures, in particular 55 °C, indicating that the impacts of cement substitutions with clay particles on cement hydration are less sensitive under elevated temperatures.

The heat flow at the "post-peak" from the normalized heat flow curves corresponding to the conversion of AFt to AFm is shown in Fig. 7a. PC presented the heat flow of 1.1 mW/g cement at 25 °C, and it increased to 3.0 mW/g cement and 4.0 mW/g cement at 40 and 55 °C, respectively, which indicates the enhanced AFt conversion under the elevated temperatures. DsMT exhibited 9.1 %, 10.0 %, and 15.7 % lower heat flow values than that of PC at 25 °C, 40 °C, and 55 °C, respectively. Compared with the changes in the length of the induction period, a less significant impact on the conversion of AFt to AFm was observed from InCon.

Fig. 7b presents the emerging time of the first and second main heat flow peaks that are related to silicate and secondary aluminate reactions, both of which are found to be accelerated significantly (shorter time) by the incorporation of DsMT at 25 °C. When saturated sMT was incorporated, these two reactions were further accelerated, and a more significant acceleration effect was obtained from the functionalized sMTs. As expected, the two peaks were moved forward at elevated temperatures for all the groups, which also decreased the variations between the groups.

3.2. Activation energy

The modified ASTM C1074 [43] approach was conducted on the cumulative hydration heat release curves, and the fitting parameters are

Table 3
Fitting parameters of the cumulative heat release curves by the three-parameter model.

Temp (℃)	Parameters	PC	DsMT	SsMT	0.2PONPE9-SsMT	0.6PONPE9-SsMT	0.2TX100-SsMT	0.6TX100-SsMT
25	H_u*	403.23	407.71	415.74	400.62	434.99	423.98	473.36
	$\tau^{\ddagger}$	13.05	12.71	12.06	11.51	12.28	13.10	14.37
	β	0.887	0.860	0.840	0.873	0.803	0.790	0.700
	R^2	0.994	0.993	0.992	0.993	0.991	0.992	0.989
40	H_u	342.22	344.26	342.33	324.32	330.21	339.60	332.07
	τ	5.57	5.69	5.70	5.68	5.83	5.78	5.81
	β	1.470	1.445	1.436	1.502	1.442	1.423	1.484
	R^2	0.997	0.997	0.997	0.9998	0.998	0.998	0.999
55	H_u	335.11	300.08	306.18	334.46	319.05	325.20	330.93
	τ	3.71	3.96	3.91	3.89	4.05	4.41	4.40
	β	1.87	2.234	2.40	2.071	1.957	1.834	1.689
	R^2	0.999	0.998	0.999	0.998	0.999	0.997	0.998

*Unit of H_u: J/g cement; ‡unit of τ: h.

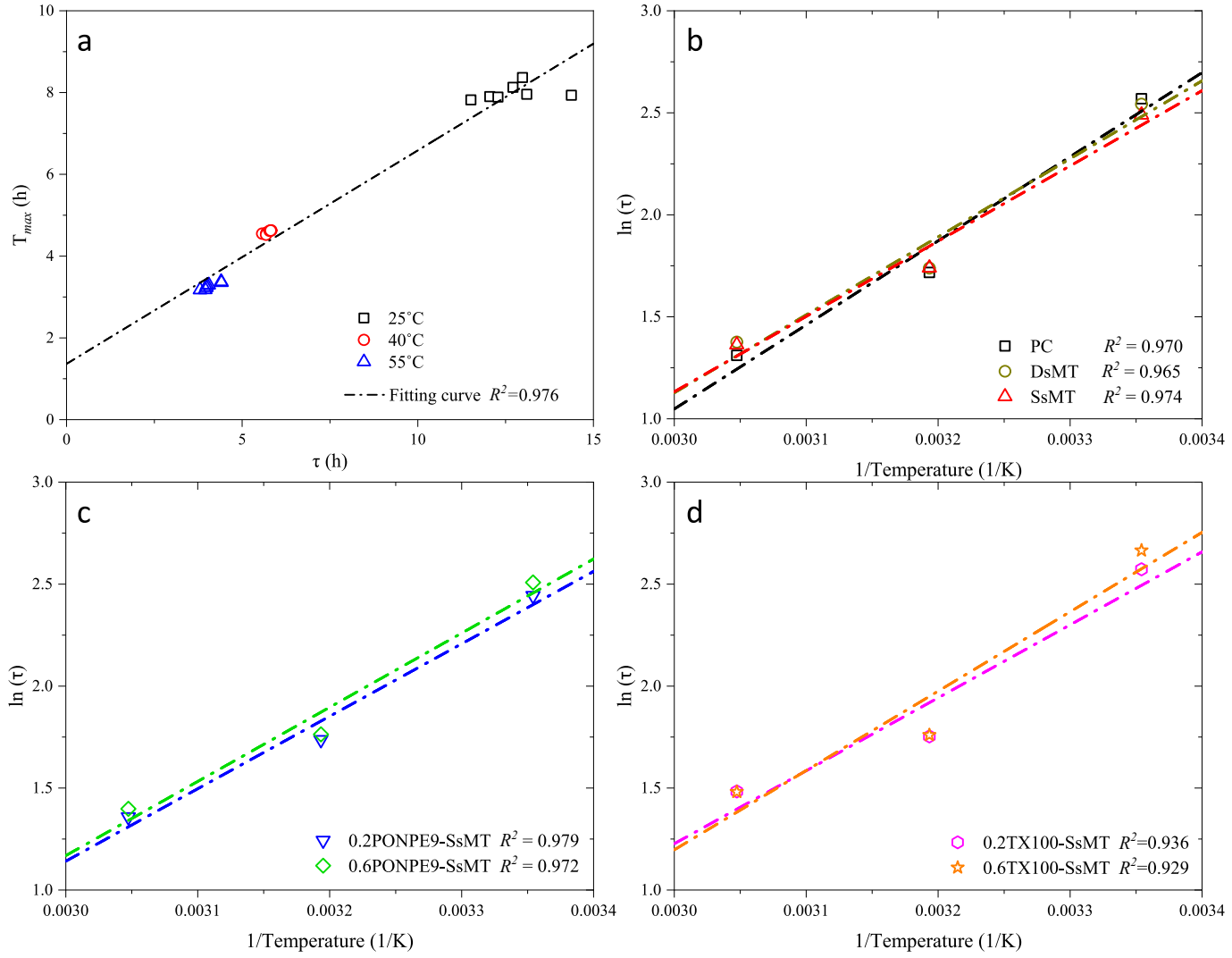

Fig. 8. (a) Correlation between τ and time to reach the maximum hydration rate from heat flow curves, and Arrhenius plot for activation energy calculation of (b) PC, DsMT, SsMT; (c) PONPE9-SsMTs; and (d) TX100-SsMTs.

presented in Table. 3. The high R^2 values over 0.99 indicate that the isothermal hydration heat data were fitted well to the three-parameter model in Eq. (1). The ultimate DOH of cement and heat release rate constant (β) are theoretically temperature-independent parameters [51,56]. However, as reported by [57], denser cement hydration products would be formed at higher temperatures, which results in the generation of a hydration "shell" around the hydrating grains acting as an impeder for the diffusion of the ions, thereby reducing the ultimate

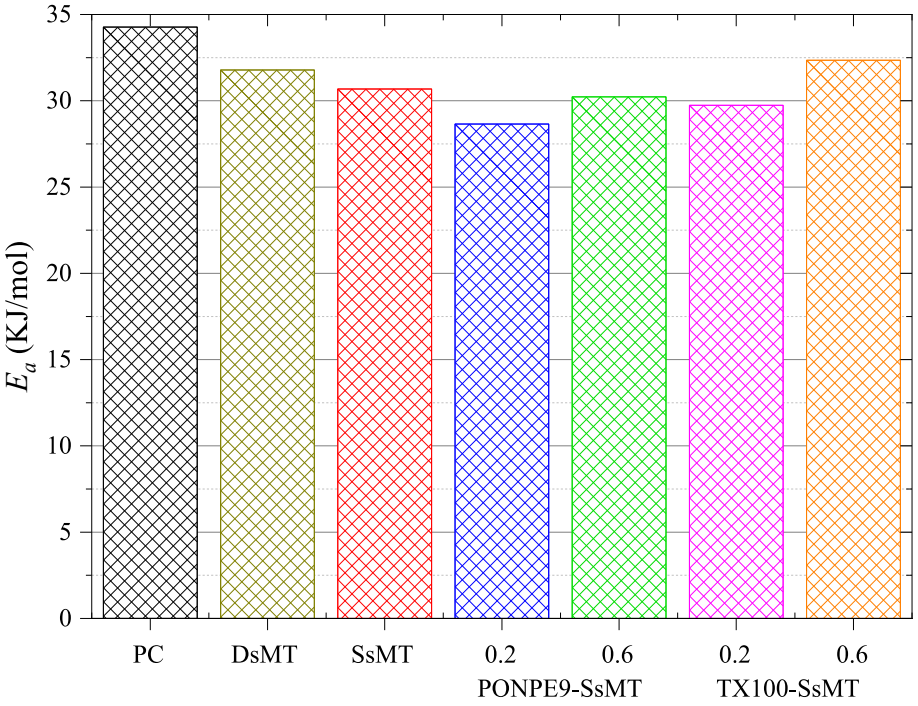

Fig. 9. Apparent activation energy of the cement hydration based on Arrhenius fitting.

DOH. As mentioned above, τ and β represent the hydration time parameter and hydration rate constant, respectively. A larger τ value means a more significant delay in hydration, while a larger β value denotes a higher hydration rate at the linear portion of the hydration curve [58]. In this study, all the three parameters (H_u, τ, and β) are modeled at three different temperatures to obtain a precise prediction.

At 25 °C, the H_u values of the binary blends containing raw and functionalized sMTs are higher than that of PC, except for 0.2PONPE9-SsMT, which showed a slightly lower value. 0.6TX100-SsMT showed 17.9 % and 13.9 % higher H_u than the PC and SsMT groups, respectively. The increased H_u values indicate higher DOH of cement in the presence of raw and functionalized sMTs. However, decreased H_u values were obtained from all the groups at elevated temperatures. At 55 °C, PC exhibited the highest H_u value among all the groups. This might be due to the temperature sensitivity of the hydration of neat cement and the dense microstructure yielded in the presence of sMT particles induced by the high temperature. Decreased τ values were obtained from the cement blends containing sMT and PONPE9-SsMTs at 25 °C, while the incorporation of TX100-SsMTs resulted in slightly higher τ values than PC indicating the different roles of PONPE9 and TX100 functionalized sMTs in accelerating or retarding cement hydration. As shown in Fig. 8a, the values of τ are positively related to the time to reach the maximum hydration rate (T_{max}) from the heat flow curves. At higher temperatures of 40C and 55 °C, lower τ values were exhibited by the cement blends, which is consistent with the increased cement hydration rate. Different from the case at 25 °C, the binary blends containing either raw or functionalized sMTs yielded higher τ than PC, indicating that the cement hydration was retarded by the incorporation of these clay particles at elevated temperatures, especially the functionalized sMTs, due to the structure densification (see the analysis below). In contrast to τ, higher β values were obtained at higher temperatures, which is expected as the hydration rate is normally considered positively correlated to the curing temperature. With increasing temperature, the binary groups containing either raw or functionalized sMTs showed more significant increases in β values than the PC indicating more considerable improvements in hydration rate at the linear portion of the hydration curves, while the TX100-SsMT groups showed lower values than PC even at 55 °C.

Fig. 8b–8d show the Arrhenius linear fitting of $\ln(\tau)$ versus $1/T$ for all the groups with R^2 values higher than 0.93. From Fig. 8b, it can be seen that the slope of PC decreases when the dry and pre-saturated sMTs were incorporated. Further decreased slopes of the fitting lines were observed in 0.2PONPE9-SsMT and 0.2TX100-SsMT, while slope values higher than SsMT were obtained from the 0.6PONPE9-SsMT and 0.6TX100-SsMT indicating the influence of surfactant's dosage in controlling sMT's role in cement hydration. This provides an indirect indication of the development of the E_a, which is calculated by multiplying the Arrhenius fitting slope with the natural gas constant.

E_a is normally defined as the potential energy barrier between the reactants and products for a reaction system, and it is widely used to evaluate the temperature sensitivity and catalytic effect of substances in cement hydration [59]. The term "apparent *Ea*" is normally employed to account for the composite nature of cement hydration, which consists of a series of simultaneous and coupled reactions [51]. As shown in Fig. 9, PC exhibited an E_a value of 34.3 KJ/mol, which agrees well with the previous studies [51,60,61] with similar testing periods and temperature ranges. With the incorporation of 3 wt% dry sMT, the E_a value decreased to 31.8 KJ/mol, while in the presence of the same amount of saturated sMT, E_a was further decreased to 30.7 KJ/mol, indicating the decreased minimum amount of energy required for triggering cement hydration [62] and the corresponding acceleration effects induced by sMT-based InCon [63]. More interestingly, the InCon based on functionalized sMTs at 0.2 CEC resulted in lower E_a values than PC, DsMT, and SsMT groups. 0.2PONPE9-SsMT exhibited the lowest E_a value of 28.7 KJ/mol, which is 16.4 % and 6.6 % lower than PC and SsMT, respectively. Although 0.2TX100-SsMT presented 3.8 % higher E_a than 0.2PONPE9-SsMT, it is still 13.2 % and 3.1 % lower than PC and SsMT, respectively. This indicates that a lower cement hydration threshold was yielded in the presence of InCon with the saturated functionalized sMT. The decreased E_a due to the functionalized sMT-based InCon might be attributed to the following reasons that can promote and accelerate the cement hydration: (1) the additional nucleation sites provided by the fine functionalized sMT particles, (2) the improved pozzolanic reactivity of sMT after the functionalization that has been confirmed by the authors' previous study [37], and (3) the extra InCon water carrying and releasing capacity of the functionalized sMTs. When the surfactant CEC was increased to 0.6, 0.6PONPE9-SsMT and 0.6TX100-SsMT yielded E_a

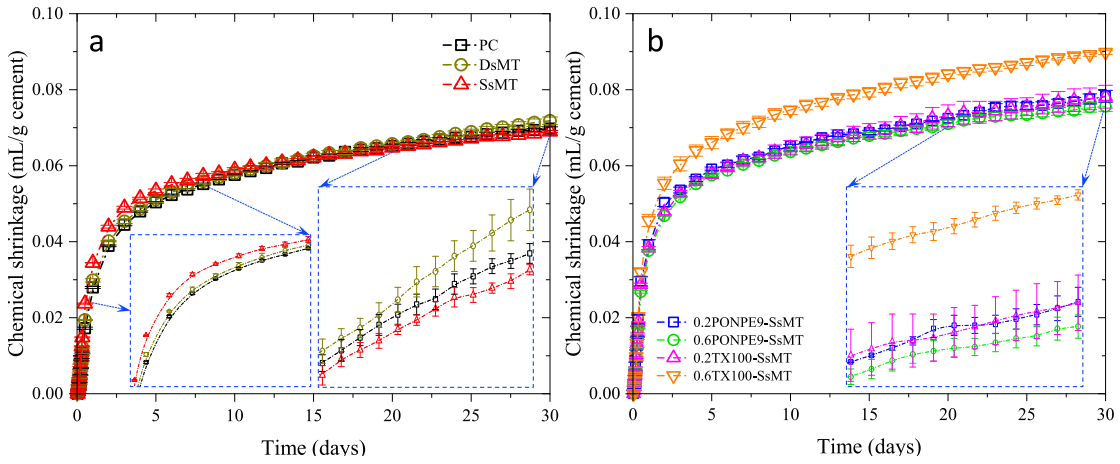

Fig. 10. Chemical shrinkage of cement pastes containing raw or functionalized sMTs.

of 30.2 and 32.4 KJ/mol, respectively, which are 5.5 % and 8.8 % higher than the ones containing the InCon with functionalized sMT at 0.2 CEC, although still 11.8 % and 5.6 % lower than PC. This again indicates the decreased effectiveness of the sMT functionalized with a higher surfactant dosage in enhancing cement hydration and the increased temperature sensitivity.

3.3. Chemical shrinkage

Fig. 10 illustrates the development of chemical shrinkage as a function of hydration time up to 30 days. Chemical shrinkage is caused by the differences in volumes between the initial reactants and the final hydration products as the products are normally denser than the reactants [64] so it can be employed to evaluate the hydration kinetics of cement under the same curing conditions. From Fig. 11a, it can be seen that PC showed a sharp and almost linear increase of chemical shrinkage during the first 8 h, and then kept increasing with a reduced shrinkage rate. After 5 days, PC yielded a chemical shrinkage of 0.05 mL/g cement, followed by a slowly increasing period up to the end of the test (30 days) with an ultimate chemical shrinkage of 0.07 mL/g cement, which is 40 % higher than that at 5 days. In the presence of dry sMT, a slightly increased chemical shrinkage was obtained. A further increased chemical shrinkage was observed from SsMT during the first 12 days, which is 1.2 % higher than PC. This chemical shrinkage evolution, however, was converted and SsMT showed a comparable chemical shrinkage with PC, which is 4.2 % lower than DsMT after 30 days. This indicates that, without functionalization, enhancement in cement hydration can be achieved from the saturated sMT, while their role is limited in the early-age hydration reactions. In addition, the development of chemical shrinkage was found not in a perfect reverse correlation with the apparent activation energy as observed from previous studies. This might be due to the fact that the shrinkage behavior of the cement-sMT composites might also be affected by the volume change of sMT and the modification of hydration products. Due to hydroscopic swelling, the saturated sMT in SsMT has a larger volume than the dry sMT and cement at the starting point of the shrinkage test. Due to the enhanced reactions between sMT and cement in the present of the extra water, the efficient consumption of the saturated sMT can result in a more significant shrinkage at early ages to form packed stable Al-rich phases, which exhibited a lower shrinkage than PC and DsMT at later ages. However, the dry sMT in DsMT experienced a lower reaction rate, and its swelling in the presence of water and consumption that resulted in volume shrinkage occurred later than that in SsMT, which might be the reason for the higher chemical shrinkage of DsMT after 15 days.

In line with the calorimetry results, significant increases in chemical shrinkage were detected from the groups with InCon based on the functionalized sMTs. 0.2PONPE9-SsMT showed a 3.5 % higher chemical shrinkage than 0.6PONPE9-SsMT after 30 days, and it is 12.2 % and 13.5 % higher than that of PC and SsMT, respectively. However, different from the calorimetry data, 0.2TX100-SsMT presented the same chemical shrinkage as 0.2PONPE9-SsMT, while a much higher chemical shrinkage of 0.090 mL/g cement was yielded from 0.6TX100-SsMT after 30 days, which is 29.0 %, 30.5 %, and 19.1 % higher than the PC, SsMT, and 0.6PONPE9-SsMT, respectively. It is interesting to see that, different from the slow development of PC and cement blends containing unfunctionalized sMTs (DsMT and SsMT) after 5 days, the cement blends with the functionalized sMT-based InCon displayed a higher increasing rate at later ages. The extra water released by the functionalized sMT (see Fig. 4a) and the increased pozzolanic reactivity and CH consumption capacity of the functionalized sMT (see Fig. 4b) are believed the primary reasons for the increased chemical shrinkage. 0.6TX100-sMT exhibited the highest WUC (47.2 %) and swelling behavior among all the investigated clays, so although with a higher E_a value, its volume change during the hydration reaction is more significant than other groups. With the enhanced cement hydration induced by the extra water and pozzolanic reactions, a higher DOH can be obtained and more hydration products denser than the reactants can be formed. The pozzolanic reactions consume the parallelly distributed CH crystal plates to form additional C—S—H gel, which refines pore structures and densifies the overall microstructure of the hydrated cement matrix. These observations, in turn, explain the changes in cement hydration kinetics (H_u and τ) in the presence of functionalized sMT particles as discussed above.

3.4. Thermogravimetric analysis

Fig. 11 displays the TGA and the corresponding DTG curves of the cement pastes after 7 days, 28 days, and 90 days of hydration. The hydration products can be identified from the distinct weight losses from the TGA curves and the DTG peaks in their specific temperature ranges. The expected increases in DOH of cement and amounts of reaction products (C—S—H, ettringite, and CH) over time can be confirmed by the increased intensity of the DTG peaks between 120 °C and 170 °C and the one between 400 and 510 °C. The two characteristic two-stage DTG peaks at 260–340 °C and 350–400 °C, which increased gradually with time, indicate the formation of hydrotalcite ($Mg_4Al_2(CO_3)(OH)_{12}\cdot 4H_2O$), an Mg-Al layered double hydroxide phase, due to the small amount of magnesium and aluminum in the cement (see Table. 1). By substituting 3 wt% cement with dry sMT, the overlapped weight loss of free water (from 30 °C to 120 °C), ettringite, and C—S—H were observed to decrease at 7 days. This might be mainly due to the decreased amount of free water in the cement-sMT system. In the later ages, especially after

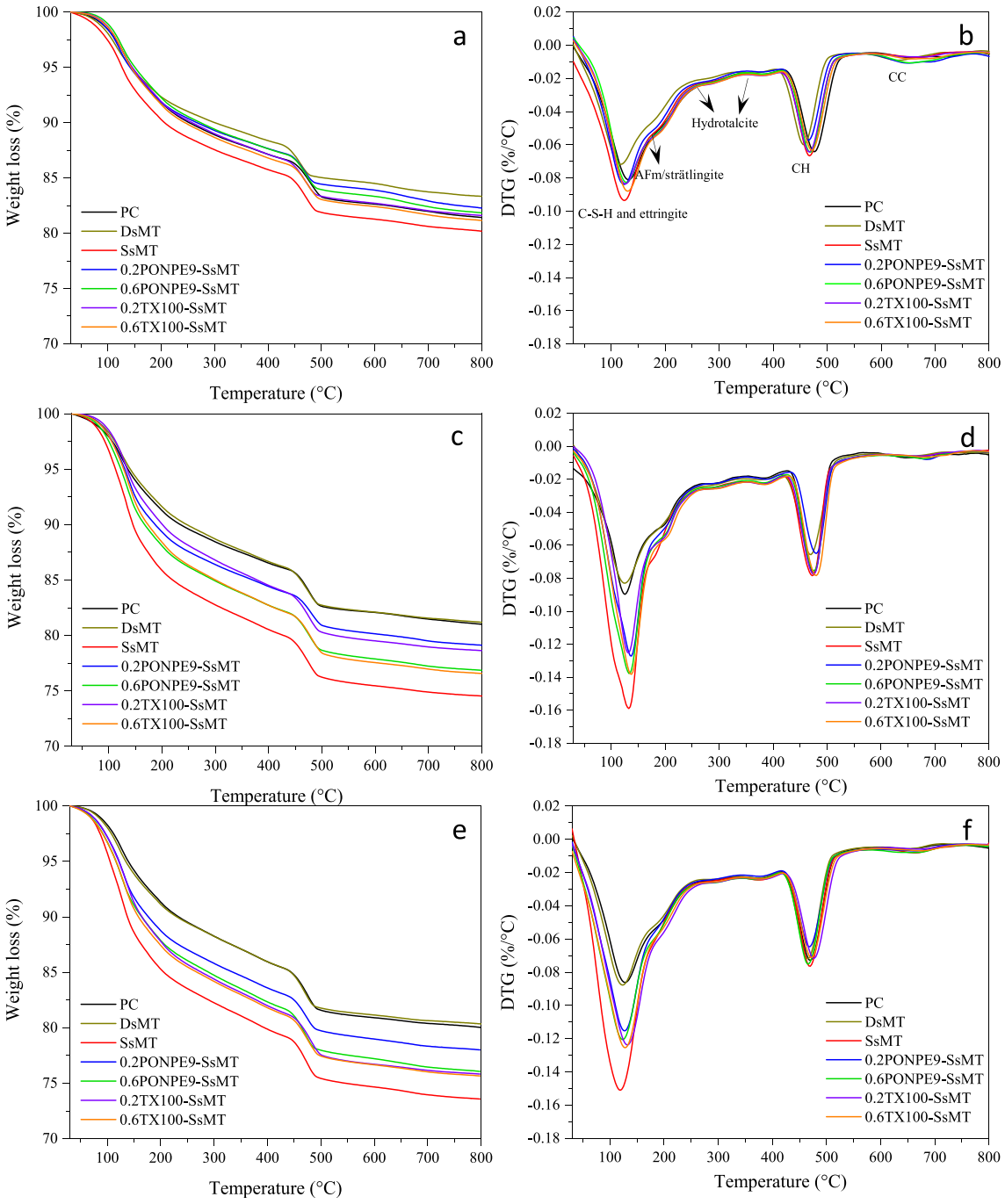

Fig. 11. TGA and DTG curves at (a-b) 7 days, (c-d) 28 days, and (e-f) 90 days.

90 days, the amounts of ettringite and C—S—H increased and exceeded that detected from PC. From SsMT, a more significant weight drop of C—S—H was observed from the TGA curve indicating the more pronounced cement hydration enhancement triggered by the extra water released from the pre-saturated sMT. The functionalized sMTs-based InCon also increased the intensity of these weight drops, while the increases are less considerable than that detected from SsMT.

Interestingly, a more significant weight loss at ~ 200 °C was observed from the cement blends containing either raw or functionalized sMTs, which might be a result of the increased amount of strätlingite formed in pozzolanic reaction induced by the amorphous aluminate in sMT. This temperature range is also shared with the decomposition of AFm, while sMT didn't exhibit a significant impact on the conversion of ettringite to AFm, and even decreased exothermic peaks were obtained (see Fig. 7). Compared with the groups containing raw sMT, the functionalized sMT groups showed a higher peak of AFm or strätlingite, demonstrating the notable and enhanced pozzolanic reactivity of the sMT after functionalization and the benefit of the gradually released water from InCon, which can be further confirmed by the increase in hydrotalcite.

Fig. 12a presents the development of CH contents of the PC and cement blends calculated from the TGA results. In PC, the gradual increase of CH was expected, as it is one of the main hydration products and normally accumulates in the cement blends with hydration time [65]. Due to the incorporation of sMT, the CH produced from cement hydration can be consumed by the pozzolanic reactions. Therefore, a CH content of 13.3 % was precipitated from DsMT after 90 days, which is 7.9 % lower than the PC group. A 5.8 % higher 90-day CH content over

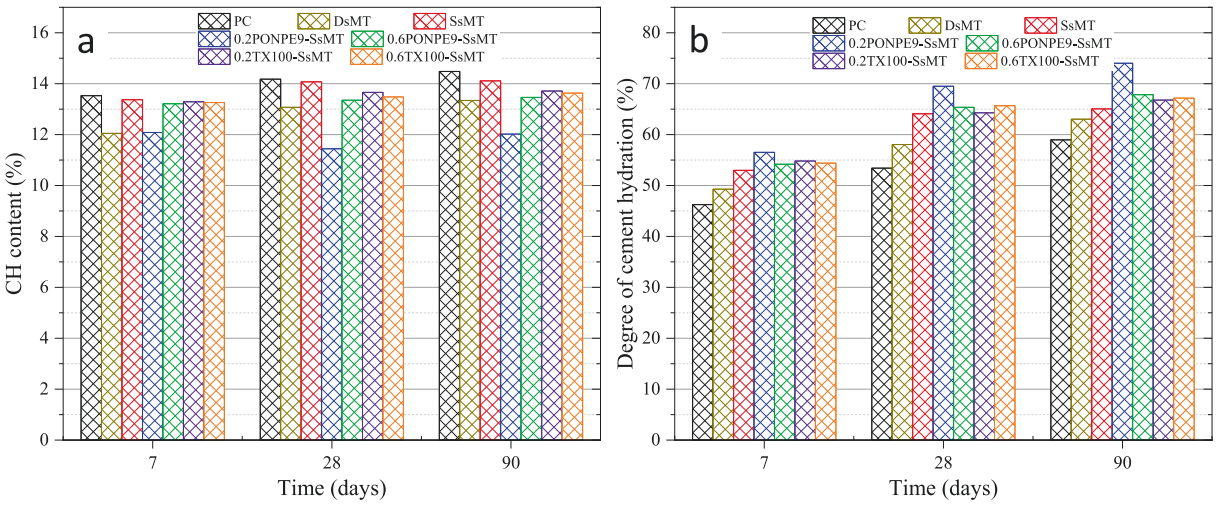

Fig. 12. (a) CH contents and (b) DOH of cement calculated from the TGA curves.

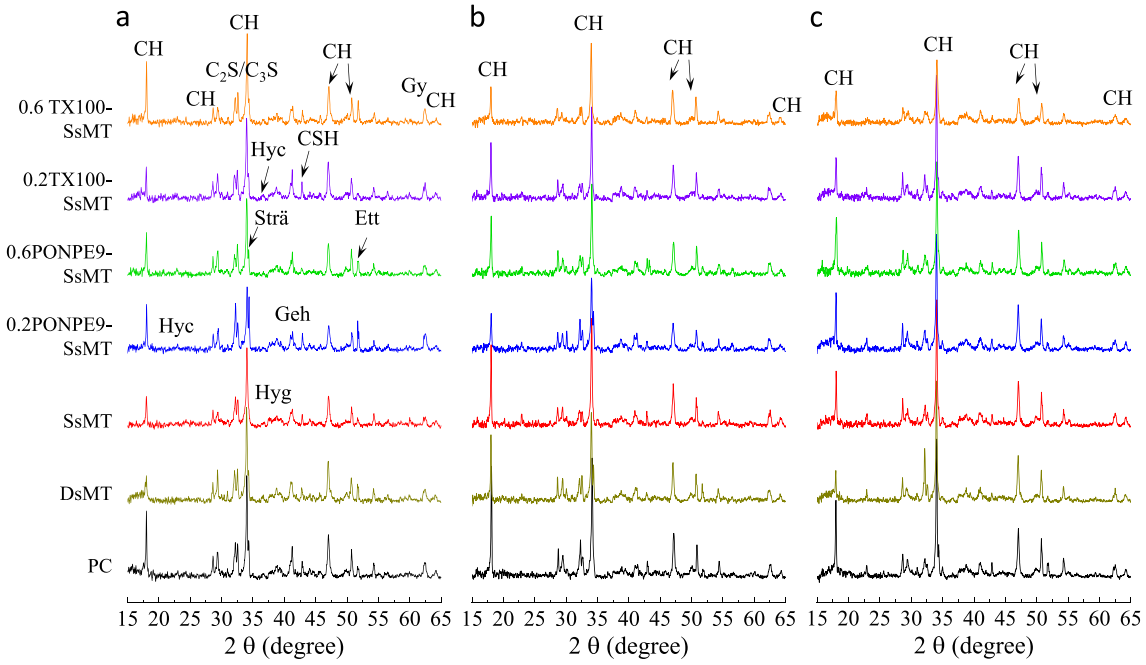

Fig. 13. XRD patterns of cement pastes after (a) 7 days, (b) 28 days, and (c) 90 days. CH: calcium hydroxide; Ett: ettringite; Strä: strätlingite; CSH: calcium silicate hydrates, Hyg: hydrogarnet; Hyc: hydrotalcite; Geh: gehlenite.

DsMT, however, was obtained when the sMT was pre-saturated, while it is still 2.6 % lower than the PC group. In the presence of functionalized sMT-based InCon, due to the enhanced pozzolanic reactivity, the CH content was further decreased. 0.6TX100-SsMT showed slightly lower CH contents than 0.2TX100-SsMT during the whole testing period, which reached 13.71 % and 13.63 % after 90 days, respectively, indicating the slightly higher pozzolanic reactivity of 0.6TX100-SsMT than that of 0.2TX100-SsMT. Compared with the sMT functionalized with TX100, PONPE9 displayed a more effective role in enhancing sMT's pozzolanicity, and a lower dosage at 0.2CEC resulted in a higher CH consumption ability. With the pozzolanic reaction proceeded, the continuous CH consumption resulted in a further decreased CH content to 11.44 % after 28 days. After 90 days, the CH content of 0.2PONPE9-SsMT increased back to 12.04 %, which might be due to the dynamic balance between the continuous formation of CH as cement hydration proceeded and the CH consumption in pozzolanic reactions. Nevertheless, 0.2PONPE9-SsMT still yielded the lowest CH content among all the tested groups. This indicates the most pronounced pozzolanic reactivity of the sMT functionalized with 0.2CEC PONPE9, which is consistent with the lime consumption test from the authors' previous study [37].

Contrary to the evolution of CH, as shown in Fig. 12b, PC exhibited the lowest DOH among all the testing ages. By incorporating 3 wt% dry sMT, the DOH was increased to 49.3 %, 58.1 %, and 63.1 % at the corresponding testing ages. After 90 days, a DOH of 65.0 % was obtained from SsMT, which is 1.9 % and 6.0 % higher than that of DsMT and PC groups, respectively. Thus, the high CH contents of SsMT observed in Fig. 12a are probably due to the enhanced cement hydration in the presence of the extra water released from the saturated sMT particles, which promotes the formation of additional CH outperforming the CH consumption of the pozzolanic reactions. The groups containing InCon with the functionalized sMTs showed further improved DOHs and the contest between the enhanced cement hydration and pozzolanic reactions in determining CH content was reversed. Among all the groups, 0.2PONPE9-sMT presented the highest DOHs of 56.5 %, 69.5 %, and

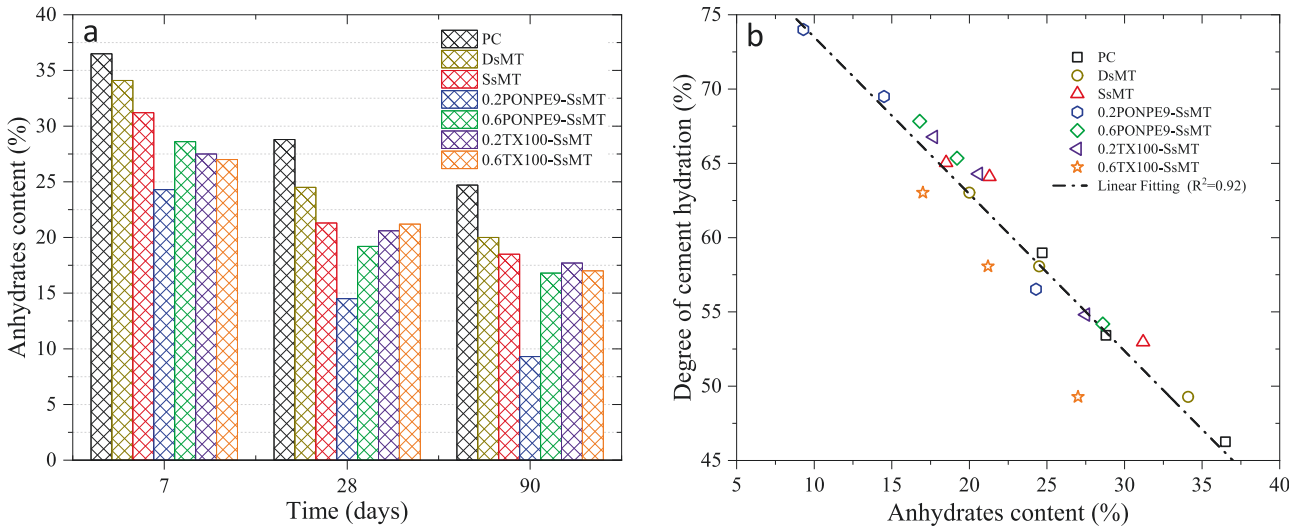

Fig. 14. (a) Development of unhydrated phases (alite and belite) contents quantified by XRD Rietveld refinement and (b) the correlation between the unhydrated phase contents and the DOH of cement.

74.1 % after 7 days, 28 days, and 90 days, respectively, indicating the most significant cement hydration enhancement. 0.6PONPE9-SsMT, 0.2TX100-SsMT and 0.6TX100-SsMT presented similar cement DOHs, which are around 67.0 % after 90 days. While these values are lower than that obtained from 0.2PONPE9-SsMT, they are higher than PC and the cement blends with untreated sMT particles (DsMT and SsMT).

3.5. X-ray diffraction analysis

Fig. 13 presents the XRD diffractogram of the hydrated cement pastes after 7 days, 28 days, and 90 days. The evolutions of the main hydration products including CH, ettringite, C—S—H, hydrogarnet, strätlingite, hydrotalcite, gehlenite, non-hydrated clinkers (C_2S/C_3S), and gypsum can be identified from their characteristic XRD peaks. Portlandite was found as the most pronounced phase showing multiple peaks at 18°, 28.5°, 34°, 47°, 50.66°, 54°, and 64.2° 2θ. As mentioned above, the CH precipitation is related to the DOH of cement and its consumption in pozzolanic reactions. In line with the TGA results, a gradual increase in CH with hydration time was observed from PC. The increasing peaks of C—S—H (42.78° and 32.17° 2θ) and ettringite (50.19° 2θ) and decreasing C_2S/C_3S and gypsum peaks at 32.61° and 62.47° 2θ, respectively, were also detected from PC with increasing DOH of cement over time.

A significant difference between PC and the cement-sMT blends lies in the decreased CH peak intensity, which shares the same trend as the TGA results indicating the CH consumption due to the desirable pozzolanic reaction that occurred in the presence of the sMT. What also agrees with the TGA data is the evolution of CH in the cement blends.

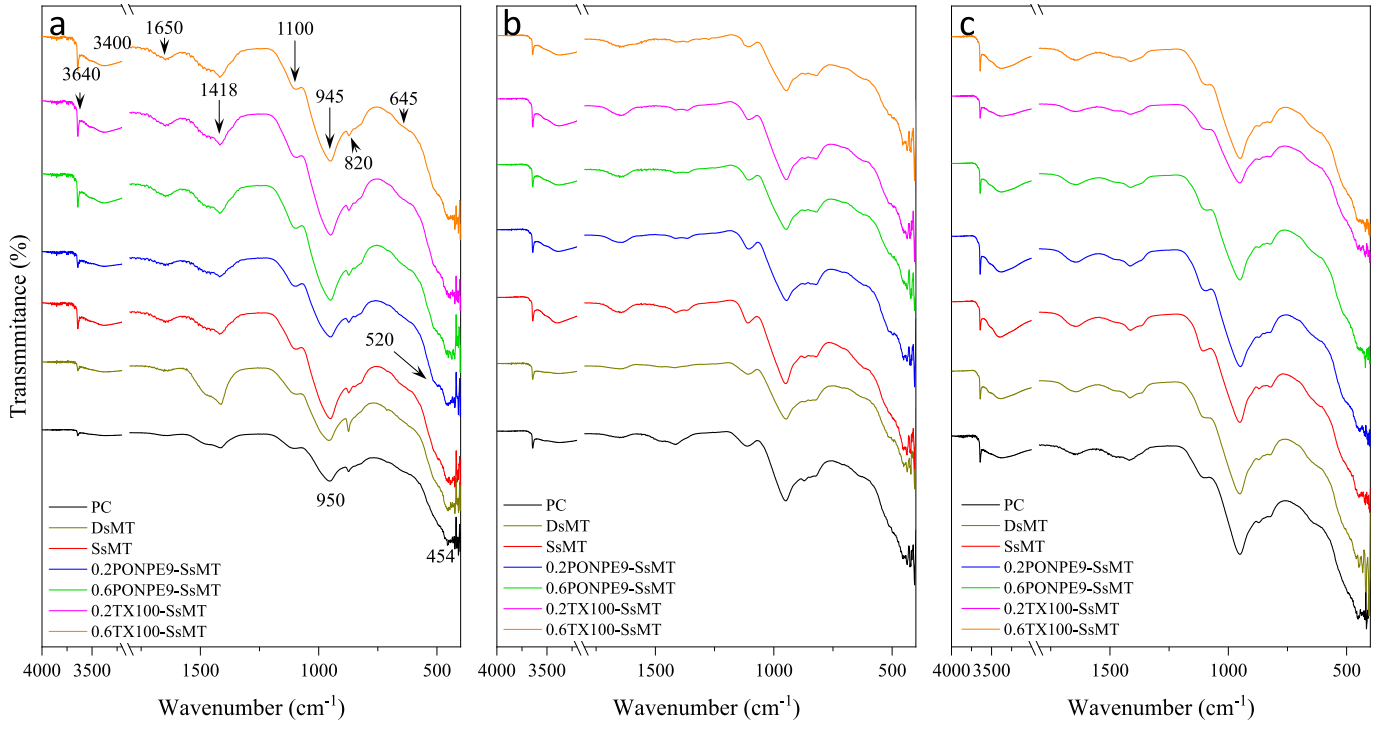

Fig. 15. ATR-FTIR spectra of the hydrated cement pastes at (a) 7 days, (b) 28 days, and (c) 90 days.

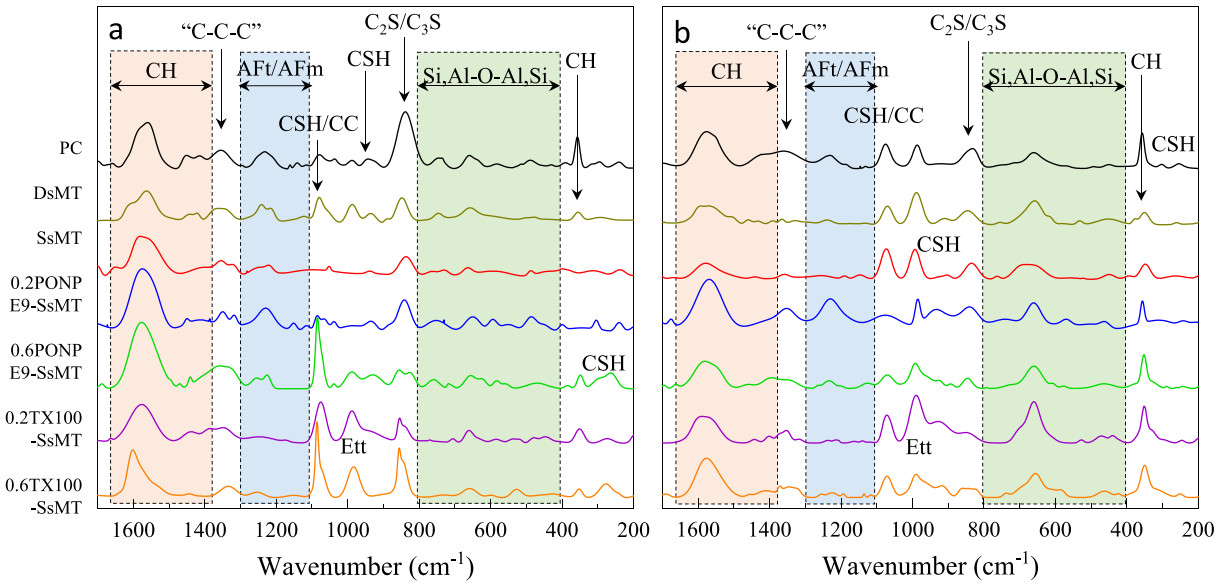

Fig. 16. Raman spectra of cement pastes at (a) 7 days and (b) 90 days.

When the sMT was pre-saturated, the CH peaks were higher than that in DsMT but still lower than the PC group. It should be noted that the C_2S/C_3S and gypsum peaks from SsMT are much lower than that detected from DsMT providing evidence for the higher DOH of cement triggered by the extra water introduced by the saturated sMT particles. The peaks for Al-containing hydration products, such as strätlingite (C_2ASH_8) at 34° 2θ, hydrogarnet (C_3AH_6) at 36.59° 2θ, and hydrotalcite ($Mg_4Al_2(CO)_3(OH)_{12}{\cdot}4H_2O$) at 22.9° and 33.94° 2θ, which resulted from the pozzolanic reaction between CH and Si-/Al-rich phases in sMT, were found to increase in the presence of dry sMT. Interestingly, although higher CH peaks were observed from SsMT, more C—S—H and Al-containing hydration products than DsMT was also detected from SsMT. These observations validate the discussion above that the increased CH in SsMT is not due to low pozzolanic reactivity but both the hydration of cement and pozzolanic reactions were enhanced by incorporating the pre-saturated sMT into the cement blends. It is just due to the fact that, without functionalization of sMT, the InCon can enhance the hydration of cement (CH production) more efficiently than the improvement of pozzolanicity of sMT. Compared with the SsMT group, further increased DOH of cement and pozzolanic reaction were unveiled by the higher peak intensities of C—S—H, strätlingite, and hydrogarnet, and the lower C_2S/C_3S and CH peaks from the groups containing saturated functionalized sMTs at each age. Among all the functionalized sMTs, it should be noted that 0.2PONPE9-SsMT presents the highest pozzolanic reactivity, in which the lowest CH peaks but the highest C—S—H (C-(A)-S—H)-related peaks were detected.

Fig. 14a shows the development of the unhydrated alite and belite quantified via the Rietveld refinement analysis. Agreeing well with the development of cement DOH determined via TGA (see Fig. 12b), the amounts of the remained anhydrates in the cement systems decreased in the presence of sMT. The benefit of InCon can be first observed from the comparison between SsMT and DsMT, where a 1.5 % lower unhydrated phase content was obtained in SsMT after 90 days of hydration. This is especially the case for 0.2PONPE9-SsMT with an alite + belite content of 9.3 % after 90 days, which is 15.4 % and 9.2 % lower than that of PC and SsMT, respectively. Compared with PC, 7.0 % and 7.7 % lower unhydrated phases remained in 0.2TX100-SsMT and 0.6TX100-SsMT after 90 days, respectively. Fig. 14b illustrates a linear correlation between the anhydrate content quantified by XRD and the DOH of cement calculated from TGA. Among the investigated groups, due to InCon, 0.2PONPE9-SsMT showed the lowest content of anhydrates and the highest DOH of cement with values of 9.3 % and 74.0 %, respectively, while the highest anhydrate content of 36.5 % and the lowest DOH value of 46.3 % were yielded by PC. This agreement again indicates the enhanced cement hydration in the presence of InCon.

3.6. ATR-FTIR spectroscopy

The ATR-FTIR spectra of the cement blends after 7 days, 28 days, and 90 days are shown in Fig. 15a, 15b, and 15c, respectively. The evolution of hydration products over time caused by the incorporation of SsMTs can be uncovered by the progression of various peaks identified from these spectra. The O—H stretch vibration in CH at ~3640 cm^{-1} [66] was observed to increase with the hydration time in both PC and DsMT, while DsMT exhibited lower peak intensity in the later ages (i.e., 28 and 90 days). Increases in the peaks associated with Si-O stretching (~950 cm^{-1}) and bending vibration (~454 cm^{-1}) of C—S—H [67,68] over time were also observed. Compared to PC, DsMT showed higher C—S—H peaks and lower CH peaks, especially after 90 days of hydration, revealing the enhancement of cement hydration and the pozzolanic reactions in the presence of sMT. A new peak at ~820 cm^{-1} attributed to the asymmetric stretching vibration of Si-O-Si or Si-O-Al bonds [69] was found in DsMT, which indicates the coexistence of C—S—H and C-A—S—H resulting from the pozzolanic reactions triggered by dry sMT. When changing dry sMT to saturated sMT, CH, C—S—H, and C-A—S—H peaks higher than that in both PC and DsMT were observed at 7 days, indicating the positive role of the extra water released by sMT in modifying the hydration reactions. After 28 days, lower CH-related peaks were observed from SsMT, but they increased again after 90 days suggesting the dynamic contest between the improved cement hydration and pozzolanic reactions.

Compared to SsMT, both the CH and C—S—H/C-A—S—H peaks increased dramatically when the pre-saturated functionalized sMTs were incorporated. This is a result of the more pronounced enhancements of cement hydration and pozzolanic reactions triggered by the InCon with functionalized sMTs. It should be noted that 0.2PONPE9-SsMT exhibits a distinct hydration product evolution from other groups. At 7 days, the lowest CH peak was detected from 0.2PONPE9-SsMT, which is consistent with the observations from TGA. After 28 days and 90 days, 0.6PONPE9-SsMT and the two TX100-SsMT groups presented comparable evolution of CH-related peaks as SsMT, i.e., the CH peaks decreased from 7 days to 28 days and then increased thereafter. 0.2PONPE9-SsMT, however, showed a gradual increase in CH-related peaks during the whole testing period indicating the most

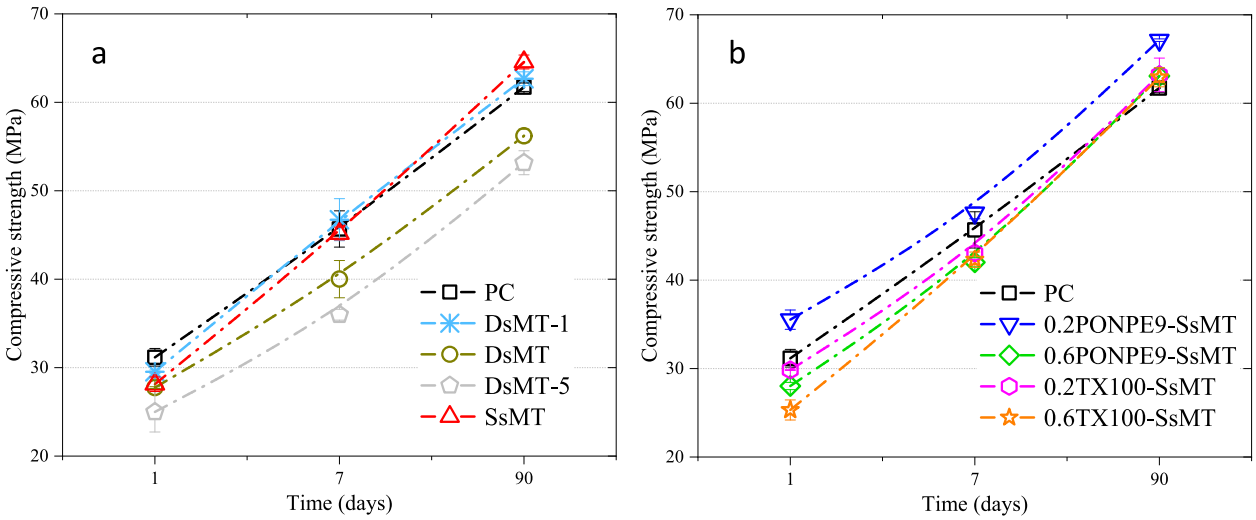

Fig. 17. Compressive strength developments of mortars: (a) the control group and the groups containing raw sMT and (b) the cement blends with InCon based on saturated sMTs after functionalization.

pronounced cement hydration enhancement. The highest C—S—H/C-A—S—H—related peak and the lowest CH peak (especially in the later ages, i.e., 90 days) in 0.2PONPE9-SsMT agree well with the TGA and XRD results, which further confirms the superior role of the InCon in sustaining both cement hydration and pozzolanic reactions.

The Ca/Al-OH bending mode (~645 cm^{-1}) and sulfates (SO_4^{2-}) vibrations (~1100 cm^{-1}) allocated to the formation of ettringite [70], the intensity of which increasing with time was detected from PC. In the binary blends, decreased ettringite-related peaks were observed, which is consistent with the XRD analysis. In the presence of sMTs, a new shoulder at around ~ 520 cm^{-1}, which indicates the formation of strätlingite [71] or C-A-H [72] from the pozzolanic reaction, appeared and increased over time. The peaks at ~3400 cm^{-1} and ~1650 cm^{-1} caused by the bending vibration of the irregularly bound or absorbed water [66,73] were observed from all the investigated groups, while relatively higher water molecule peaks than PC and DsMT were observed from the blends containing saturated raw or functionalized sMT particles. This is particularly a case for early ages (7 and 28 days), which is due to the extra water introduced by InCon.

3.7. Raman spectroscopy

Fig. 16a and 16b depict the Raman spectra of the powdered cement pastes after 7 days and 90 days of hydration. From the spectra, the stretching vibration of –OH at ~356 cm^{-1} and the range of 1400–1700 cm^{-1}, the C—S—H/C-A—S—H phases between 400 cm^{-1} and 800 cm^{-1}, the ettringite bands at ~985 cm^{-1}, and the vibration of SO_4^{2-} from the sulfate phases (AFt/AFm) in the range of 1100–1300 cm^{-1} can be identified. As the hydration proceeded, the intensity of these hydration product peaks increased from 7 days to 90 days in PC, while the non-hydrated C_2S/C_3S at around ~832 cm^{-1} decreased with time. When 3 wt% dry sMT was incorporated into the cement blends, the decreased CH peaks along with the increased C—S—H/C-A—S—H related peaks were observed revealing the desired CH consumption and its conversion into C-(A)-S—H binding phases in pozzolanic reaction. When the sMT particles are saturated with water, higher CH and C—S—H peaks were exhibited at 7 days. While the CH peaks of SsMT became lower than that of DsMT after 90 days, higher C—S—H and C-A—S—H—related peaks and lower unhydrated C_2S/C_3S peaks, which are in agreement with the TGA, XRD, and ATR-FTIR analysis above, were obtained from SsMT indicating the effectively enhanced pozzolanic reactions triggered by the gradually released water.

The most marked decrease in CH peaks and the lowest C_2S/C_3S peaks from 7 days to 90 days were detected from 0.2PONPE9-SsMT indicating the most enhanced CH consumption due to the high pozzolanic reactivity of the sMT functionalized with PONPE9 at 0.2 CEC and the positive role of InCon in improving DOH of cement. 0.6PONPE9-SsMT and 0.2/0.6TX100-SsMT exhibited higher CH peaks than 0.2PONPE9-SsMT, which is in line with the TGA, XRD, and FTIR data indicating less improvement in pozzolanic reactivity. It should be noted that, compared with the untreated sMT, more significantly enhanced cement hydration with the formations of additional C—S—H and C-A—S—H phases were obtained in the presence of the saturated functionalized sMTs, which might be due to their higher water-carrying capacity and further improved pozzolanicity triggered by the intercalation of surfactants [37].

3.8. Compressive strength

The development of compressive strength of the cement mortars as a function of hydration time up to 90 days is presented in Fig. 17a and 17b, respectively. In addition to the cement substitution with 3 wt% dry sMT (DsMT), the compressive strength of two groups incorporating 1 wt % (DsMT-1) and 5 wt% dry sMT (DsMT-5) were also tested. As shown in Fig. 17a, PC yielded a compressive strength of 31.2 MPa after 1 day, which decreased to 29.5 MPa, 27.7 MPa, and 25.0 MPa, respectively, after replacing 1 wt%, 3 wt%, and 5 wt% cement with dry sMT. This strength loss might be due to the predominant water absorption, poor dispersion, and high agglomeration of dry sMT particles in the cement matrix [74]. This negative impact became less significant with time, especially at the low dosage. After 7 days and 90 days, DsMT-1 showed 2.3 % and 1.5 % higher compressive strength than PC, while the 90-day compressive strength of DsMT and DsMT-5, is still 8.9 % and 13.8 %, respectively, lower than that of the PC group. Thus, when considering mechanical strength, the optimal dosage of dry sMT would be only 1 %, and it is consistent with the previous investigations [75,76]. Interestingly, although the 1-day compressive strength is still lower than PC, the incorporation of the saturated sMT particles resulted in a more considerable gain of compressive strength in the later ages. After 90 days, SsMT yielded a compressive strength of 64.6 MPa, which is 4.7 % and 14.9 % higher than that of PC and DsMT, respectively, and even 3.0 % higher than DsMT-1. This indicates that the strength loss due to the high incorporation level of sMT can be offset by InCon, which paves a path to improve the mechanical properties of concrete at a higher cement substitution level.

After functionalization, the 1-day compressive strength of

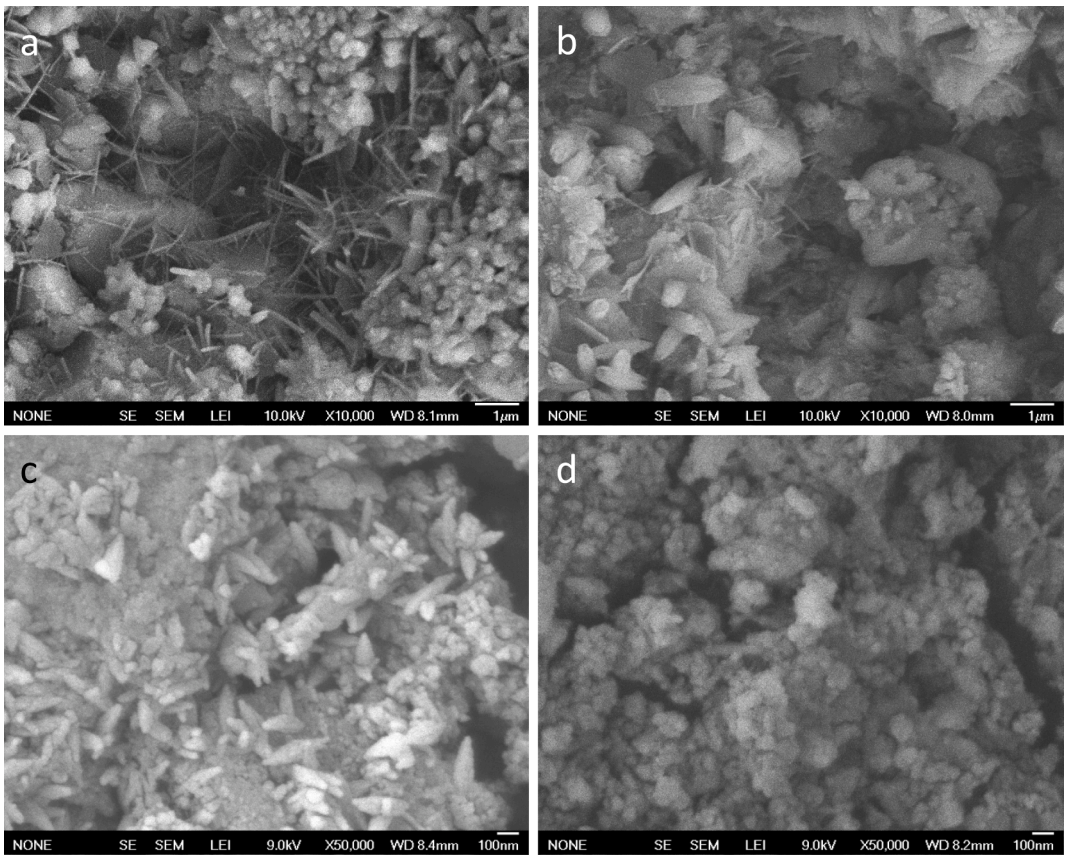

Fig. 18. SEM images of (a) and (b) PC, (c) SsMT, and (d) 0.2PONPE9-SsMT.

0.2PONPE9-SsMT and 0.2TX100-SsMT is higher than that of SsMT, while lower strength was obtained from the cement blends containing sMTs functionalized with additional surfactants (0.6PONPE9-SsMT and 0.6TX100-SsMT) (see Fig. 17b). It was found that comparable 90-day strength of around 63.0 MPa, which is 2.0 %-2.5 % higher than PC, was yielded by 0.6PONPE9-SsMT, 0.2TX100-SsMT, and 0.6TX100-SsMT. Again, 0.2PONPE9-SsMT showed the highest compressive strength during the whole testing age. After 90 days, the strength of 0.2PONPE9-SsMT increased to 67.1 MPa, which is 8.8 % and 3.8 % higher than that of PC and SsMT, respectively.

3.9. Microstructure analysis

The SEM micrographs of hydrated cement pastes at 90 days were captured to analyze the microstructures of PC, SsMT, 0.2PONPE9-SsMT, 0.6PONPE9-SsMT, and 0.6TX100-SsMT. As shown in Fig. 18a and 18b, the typical hexagonal CH sheets, needle-like ettringite crystals, and semi-crystal C—S—H phases can be observed from PC. Rice-shaped grains with an average length and width of around 1.5 μm and 0.5 μm, respectively, were detected. As reported in [77], this phase might be a unique form of secondary CH crystal clusters formed in a restrained growth space, especially after long-term hydration. In SsMT, no ettringite and fewer hexagonal CH sheets were detected (see Fig. 18c). The rice-shaped CH crystal clusters were also formed but with a smaller length and width of 0.25 μm and 0.08 μm, respectively, indicating that the incorporation of sMT can help to densify the microstructure of the cement paste. These observations are in line with the characterizations of hydration products that the pozzolanic reaction facilitates the consumption of CH, which leads to the formation of additional C—S—H phases. In 0.2PONPE9-SsMT, however, no hexagonal sheets or rice-shaped crystal clusters of CH can be detected, which is in line with the TGA, XRD, and Raman results as discussed above. Due to the integration of extra water and increased pozzolanic reaction triggered by InCon, additional C—S—H gels were produced.

As shown in Fig. 19, no ettringite needles were seen in the functionalized sMT samples (PONPE-SsMT and TX100-SsMT) as the transformation of AFt to AFm was accelerated in the presence of InCon, especially after 90 days of hydration. Due to the significant consumption of CH, the rice-shaped secondary CH crystal clusters disappeared from these InCon groups. However, hexagonal CH sheets were still observed, and 0.6PONPE9-SsMT contains more CH than 0.6TX100-SsMT, which is consistent with the phase's evolution analysis from TGA, XRD, ATR-FTIR, and Raman spectroscopy above. Although TX100 is found less effective than PONPE9 in improving the role of sMT in enhancing the early-age hydration of cement, more C—S—H gels can be detected from 0.6TX100-SsMT than 0.6PONPE9-SsMT and therefore, densify the packing of hydration products better. These microstructural observations confirmed the great potential of the functionalized sMT-based InCon in improving the cement modification efficiency of sMT.

4. Discussion

To uncover the underlying mechanisms of the functionalized sMT-based InCon in enhancing cement hydration, the correlations between clay properties after functionalization and DOH, and phase evolutions of the cement blends as well as the physical and mechanical properties of cement are elucidated and discussed. Different from the CH consumption data shown in Fig. 4, which was determined from sMT-CH blends, the CH contents determined from the sMT-cement blends are analyzed here. As shown in Fig. 20a, with the increased release of Al and Si from the functionalized sMT into the simulated pore solution, decreased CH contents were obtained from the cement blends. Reversely, a positive linear correlation between the DOH of cement and the dissolution of Al and Si from sMT particles was obtained from the cement blends

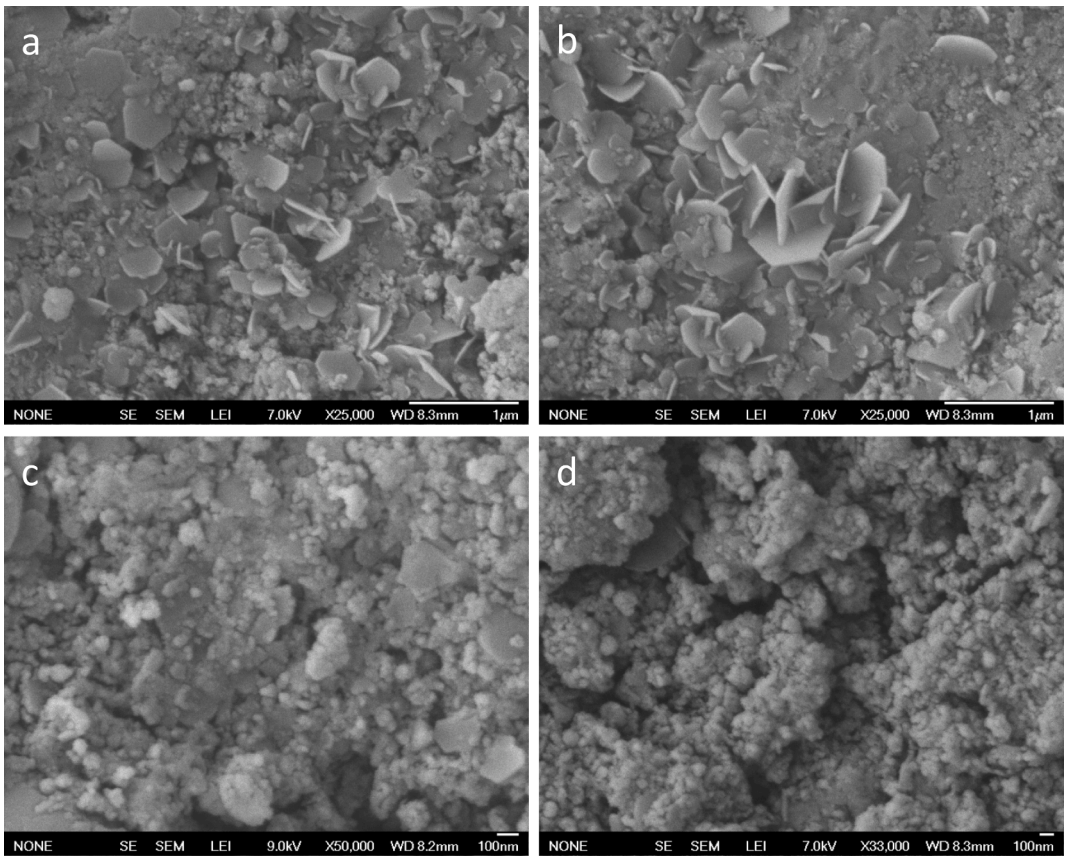

Fig. 19. SEM images of (a, b) 0.6PONPE9-SsMT and (c, d) 0.6TX100-SsMT.

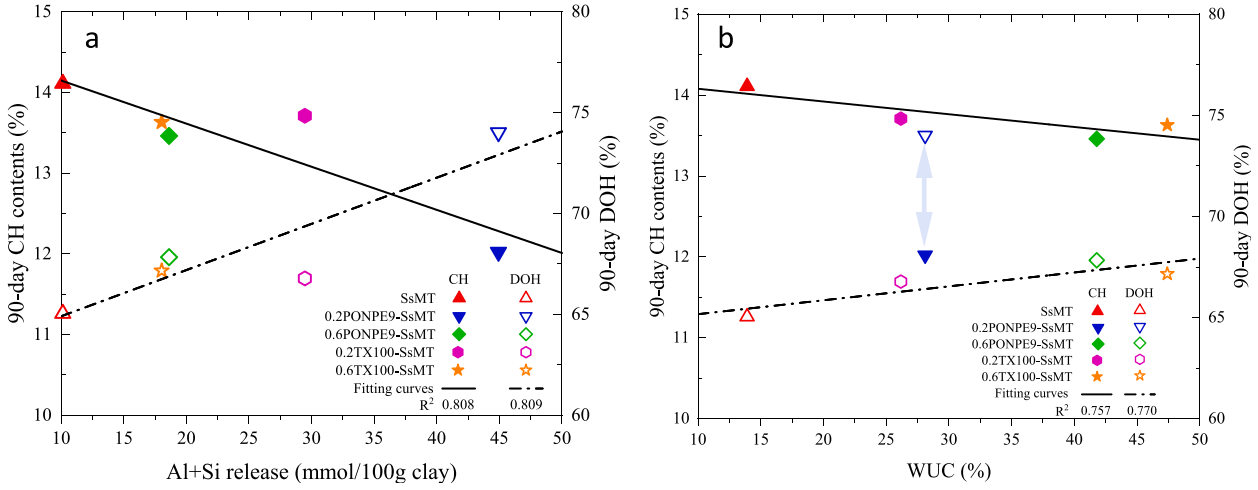

Fig. 20. (a) Correlations between Al and Si released from sMT particles in pore solution and 90-day CH contents and DOH, (b) correlations between WUC of sMT particles and 90-day CH contents and DOH of the cement blends.

indicating that sMT particles became more reactive to participate in the pozzolanic reactions and thereby enhancing the hydration of cement. In addition to the release of Al and Si from the sMT particles, the WUC before and after functionalization also determines the role of sMT in InCon. As seen in Fig. 20b, the DOH of cement is positively correlated to the WUC of the sMT particles confirming the benefit of the extra InCon water in enhancing cement hydration. After the non-ionic functionalization, more water can be absorbed by sMT, which is used as a water reservoir in the proposed InCon, thereby increasing the water carrying capacity. The ultra-fine particle size and improved dispersion of sMT after functionalization trigger the uniform distribution of this new water reservoir in the cement matrix, which can gradually release the extra water as the cement hydration proceeds. It is worth noting that the extra water released from the saturated sMT particle not only provides more available water to continue the cement hydration but also plays a positive role in enhancing the pozzolanic reactions between sMT and CH in the hydrated cement matrix. If consider cement hydration and pozzolanic reaction separately, the former will induce the formation of additional CH while the latter will consume more CH. This contest was dominated by the enhancement of pozzolanic reaction as an overall

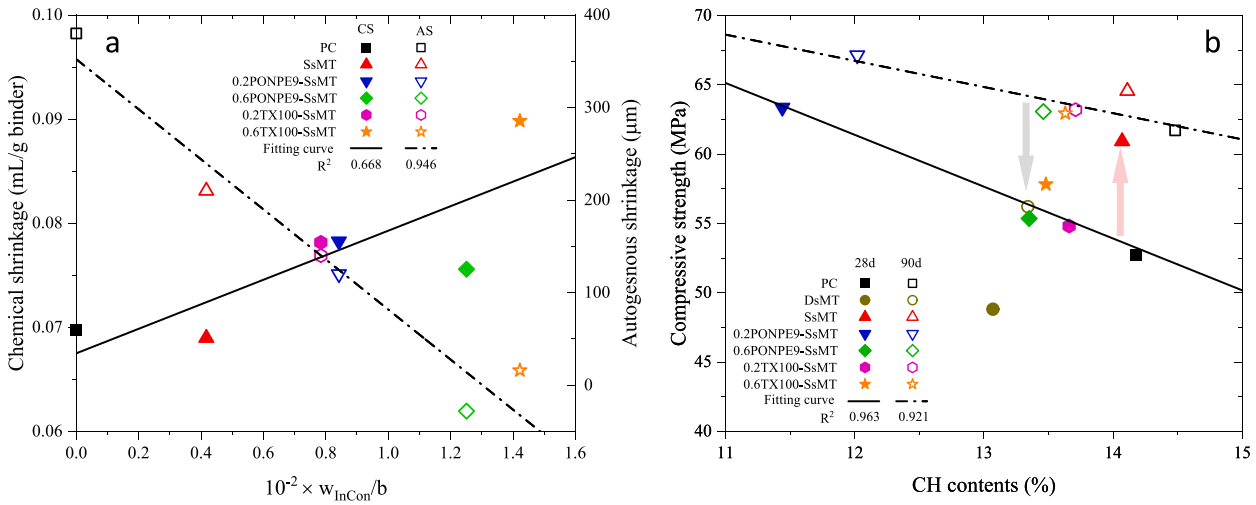

Fig. 21. (a) Correlations between InCon water to binder ratio (w_{InCon}/b) and chemical shrinkage (CS) and autogenous shrinkage (AS), (b) correlations between CH contents and compressive strength of the cement blends.

negative correlation between the WUC of sMTs and CH content was observed from the investigated cement blends. A unique group that is not on the linear correlations is 0.2PONPE9-SsMT, the CH content of which is the lowest with a higher DOH than other groups. This is in line with the pozzolanic reactivity of sMT functionalized with 0.2PONPE9 in a CH consumption test in the authors' previous study [37].

A direct result of the modified evolution of cement hydration and reaction products is the property changes of the hydrated cement composites. Fig. 21a presents the correlation between the extra water introduced by the InCon to binder ratio (w_{InCon}/b) and chemical shrinkage, and that between the w_{InCon}/b ratio and autogenous shrinkage. Different evolutions can be observed from chemical and autogenous shrinkages. A positive correlation between chemical shrinkage and the w_{InCon}/b ratio was obtained from the cement blends. As discussed above, the InCon water introduced by the pre-saturated sMT reservoirs can facilitate both cement hydration and pozzolanic reactions, which resulted in the formation of dense reaction products. The saturation of pores after the setting of the cement matrix can also result in the formation of densified microstructure [78]. Different from chemical shrinkage, the driving force of autogenous shrinkage is the change in the capillary pressure induced by self-desiccation as a balance between the absolute volume reduction (chemical shrinkage) and the building up of the capillary network [79]. It has been reported that one of the main benefits of internal curing is to diminish the autogenous shrinkage of the cement blends by maintaining a high level of humidity in pastes and relieving autogenous shrinkage [80]. The negative correlation between the 48-hour autogenous shrinkage and w_{InCon}/b ratio of the blends (see Fig. 21a) second the previous studies. A critical change was obtained from the cement blends containing sMT functionalized with PONPE9 and TX100 at 0.6CEC, in which the autogenous shrinkage was fully suppressed indicating that the improved WUC due to the enlarged basal spacing in the presence of surfactants can enable a more effective water reservoir role of sMT to resist self-desiccation.

Since CH is considered the weak point of the hydrated cement [81], with more CH reacted to form additional C—S—H phases, increased strength was obtained from the blends. As seen in Fig. 21b, a negative correlation between the CH contents and compressive strength at 28 and 90 days was observed in the groups except for DsMT and SsMT. By incorporating 3 wt% of dry sMT in the cement blends, the CH contents decreased to 13.1 % and 13.3 % after 28 days and 90 days, while the corresponding compressive strength also decreased. As discussed in Section 3.8, the lower compressive strength might be due to the poor dispersion, high agglomeration, and predominant water absorption of dry sMT particles in the cement matrix that less water is available to fuel cement hydration. In SsMT, however, 24.8 % and 4.6 % higher compressive strength than DsMT were obtained at 28 and 90 days, respectively. After functionalization, the saturated sMT, especially the 0.2PONPE9-SsMT, triggers a further decrease in CH content and an increase in strength.

5. Conclusions

A novel internal conditioning (InCon) technique tailored based on sMTs functionalized with two non-ionic surfactants (PONPE9 and TX100) was proposed in the current study. Different from conventional internal curing, InCon integrates the benefits of gradual water release and pozzolanicity in a single system. The hydration kinetics of cement with InCon, and its influence on the evolutions of phases, shrinkage, microstructure, and mechanical strength, were investigated. The following conclusions can be drawn:

(1) Both the silicate reaction and secondary aluminate reactions are accelerated and enhanced by InCon. Shortened induction period and decreased time to reach the main exothermic peaks were obtained. At elevated temperatures, further enhanced cement hydration was observed from all the groups, while the role of InCon in enhancing cement hydration becomes less significant.
(2) The heat release time parameter, τ, is positively related to the time to reach the maximum hydration rate, while lower τ values were exhibited by the cement blends at elevated temperatures. In the presence of InCon, the cement blends yielded lower and higher τ values than PC at room and elevated temperature, respectively, indicating the less effective role of InCon under high temperature due to structure densification. Increases in heat release rate constant, β, are triggered by InCon at varying temperatures indicating the improvement in hydration rate at the linear portion of the hydration curves.
(3) With InCon, the apparent activation energy of cement hydration was decreased from 34.3 KJ/mol to 28.7 KJ/mol, indicating a lower temperature sensitivity and threshold of the cement hydration process was triggered in the presence of the saturated functionalized sMT. This might be due to the additional nucleation sites, the improved pozzolanic reactivity of sMT, and the extra InCon water released by the functionalized sMT reservoirs as cement hydration proceeds.
(4) Due to the coupled benefits of the enhanced pozzolanic reactivity and increased water-reserving ability of sMT particles after functionalization, decreased CH contents, improved degree of

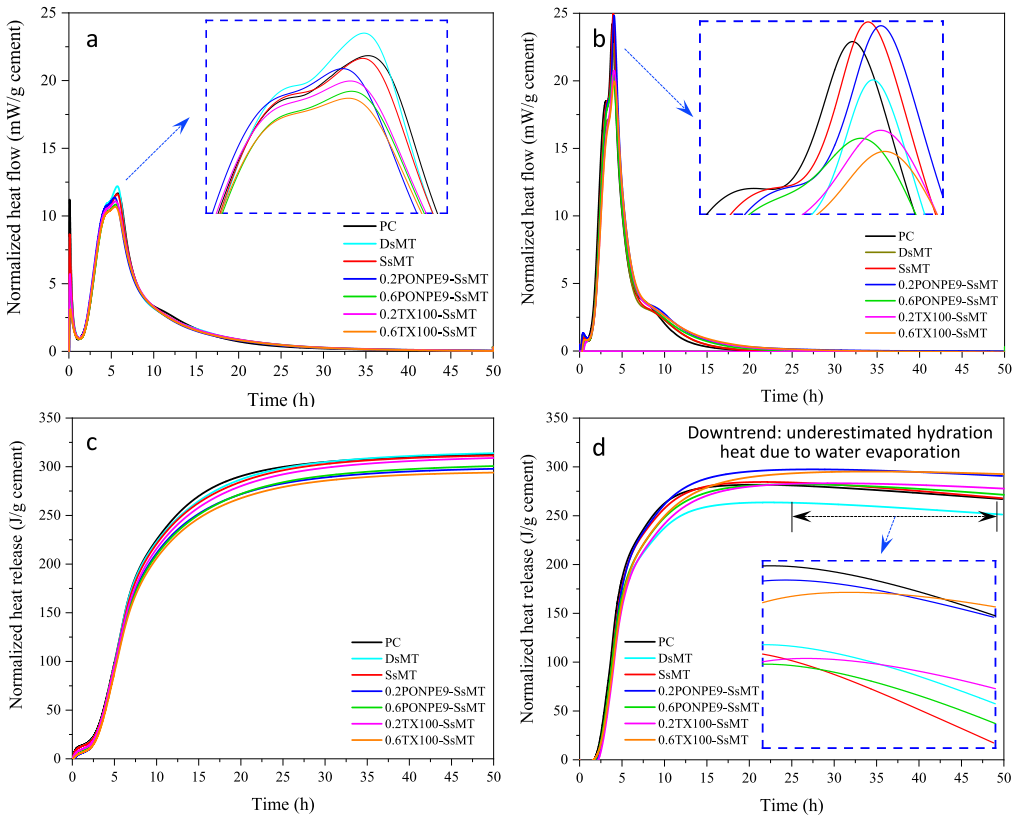

Fig. A1. Normalized heat flow at (a) 40 °C and (b) 55 °C, and normalized cumulative heat release at (c) 40 °C and (d) 55 °C before correction.

cement hydration, increased chemical shrinkage, and the formations of additional C—S—H and aluminum-containing phases were obtained from the cement with InCon. Compared with TX100, PONPE9 displayed a more effective role in enhancing sMT's pozzolanicity, and a lower dosage at 0.2CEC resulted in a higher CH consumption ability.

(5) The negative impact of dry sMT on the early age strength of cement can be offset by InCon, which paves a path to improve the mechanical properties of concrete at a higher cement substitution level. 0.2PONPE9-SsMT group yields a 90-day compressive strength of 67.1 MPa, which is 8.8 % and 3.8 % higher than the PC and SsMT groups, respectively.

(6) The hexagonal portlandite crystal and rice-shaped crystalline clusters, a secondary CH crystal formed in a restrained growth space after long-term hydration, are observed in neat PC and cement containing saturated sMT. In the presence of InCon, fewer hexagonal sheets, less ettringite, and additional C—S—H are formed densifying the microstructure of the cement matrix.

(7) The identified correlations between sMT's properties and cement hydration, as well as the physical and mechanical properties of the hydrated cement, suggest that the improved water reservation capacity and pozzolanic reactivity of sMT after functionalization and saturation are the underlying triggers of cement hydration enhancement, and the improvement of physical and mechanical properties of cement.

CRediT authorship contribution statement

Dayou Luo: Investigation, Validation, Writing – original draft. **Jianqiang Wei:** Conceptualization, Methodology, Data curation, Supervision, Writing – review & editing, Funding acquisition.

Declaration of Competing Interest

The authors declare that they have no known competing financial interests or personal relationships that could have appeared to influence the work reported in this paper.

Data availability

Data will be made available on request.

Acknowledgments

This work was supported by the United States National Science Foundation (NSF) under the award No. 1935799. The authors gratefully acknowledge the support for this project.

Appendix A. . Isothermal calorimetry data at 40 °C and 55 °C before correction

The raw heat flow and cumulative heat release curves at elevated temperatures of 40 °C and 55 °C are shown in Fig. A1. As expected, accelerated cement hydration was observed in all the groups due to the higher temperatures. The secondary aluminate reaction peak of PC was brought forward to 5.8 and 3.8 h at 40 and 55 °C, respectively, which were 2.6 and 4.4 h earlier than that at 25 °C. The peak amplitudes were also increased by 162.2 % and 426.1 % by elevating the temperature to 40 and 55 °C, respectively. It should be noted that decreased differences in the exothermic peaks in terms of occurrence time and amplitude between PC and the cement blends containing raw or functionalized sMTs can be observed under the two elevated temperatures. From the accumulative heat release curves at 55 °C, a downtrend after around 25 h was observed. As discussed above, this might be caused by the evaporation of water from the fresh cement samples under elevated

temperatures. These curves were corrected by considering the heat loss caused by water evaporation under the same elevated temperatures. The heat flow and cumulative heat release curves after correction are shown in Fig. 6.

References

[1] T.C. Powers, Structure and physical properties of hardened Portland cement paste, J. Am. Ceram. Soc. 41 (1) (1958) 1–6, https://doi.org/10.1111/j.1151-2916.1958.tb13494.x.

[2] A.M. Ley-Hernandez, J. Lapeyre, R. Cook, A. Kumar, D. Feys, Elucidating the effect of water-to-cement ratio on the hydration mechanisms of cement, ACS omega 3(5) (2018) 5092-5105https://doi.org/10.1021/acsomega.8b00097.

[3] E. Berodier, K. Scrivener, Evolution of pore structure in blended systems, Cem. Concr. Res. 73 (2015) 25–35, https://doi.org/10.1016/j.cemconres.2015.02.025.

[4] J. Lindgård, Ö. Andiç-Çakır, I. Fernandes, T.F. Rønning, M.D. Thomas, Alkali–silica reactions (ASR): Literature review on parameters influencing laboratory performance testing, Cem. Concr. Res. 42(2) (2012) 223-243https://doi.org/10.1016/j.cemconres.2011.10.004.

[5] F.S.T. Slamecka, The effect of water ratio on microstructre and composition of the hydration products of Portland cement pastes, Ceramics– Silikáty 46 (4) (2002) 152–158.

[6] T.C. Powers, A discussion of cement hydration in relation to the curing of concrete, Highway Research Board Proceedings (1948).

[7] R.J. Flatt, G.W. Scherer, J.W. Bullard, Why alite stops hydrating below 80% relative humidity, Cem. Concr. Res. 41(9) (2011) 987-992https://doi.org/10.1016/j.cemconres.2011.06.001.

[8] D.P. Bentz, P. Lura, J.W. Roberts, Mixture proportioning for internal curing, Concr. Int. 27 (2) (2005) 35–40.

[9] S. Mindess, F. Young, D. Darwin, Concrete, 2nd, Edition,, Technical,, Documents (2003).

[10] D. Cusson, T. Hoogeveen, An experimental approach for the analysis of early-age behaviour of high-performance concrete structures under restrained shrinkage, Cem. Concr. Res. 37(2) (2007) 200-209https://doi.org/10.1016/j.cemconres.2006.11.005.

[11] S. Nie S. Hu F. Wang P. Yuan Y. Zhu J. Ye Y. Liu Internal curing–a suitable method for improving the performance of heat-cured concrete Constr. Build. Mater. 122 (2016) 294–301https://doi.org/10.1016/j.conbuildmat.2016.05.159.

[12] D.P. Bentz, W.J. Weiss, Internal curing: a 2010 state-of-the-art review, US Department of Commerce, National Institute of Standards and Technology, 2011.

[13] G. Espinoza-Hijazin, Á. Paul, M. Lopez, Concrete containing natural pozzolans: new challenges for internal curing, J. Mater. Civ. Eng. 24(8) (2012) 981-988https://doi.org/10.1061/(ASCE)MT.1943-5533.0000421.

[14] T. Bremner, J. Ries, S.J. Hayde, Father of the Lightweight Concrete Industry, Concr. Int. 31 (8) (2009) 35–38.

[15] H. Kim, D. Bentz, Internal curing with crushed returned concrete aggregates for high performance concrete, NRMCA Concrete Technology Forum: Focus on Sustainable Development, MD, NRMCA Silver Spring, 2008, pp. 20–22.

[16] V. Mechtcherine, L. Dudziak, J. Schulze, H. Staehr, Internal curing by super absorbent polymers (SAP)–Effects on material properties of self-compacting fibre-reinforced high performance concrete, Int RILEM Conf on Volume Changes of Hardening Concrete: Testing and Mitigation, Lyngby, Denmark (2006) 87–96.

[17] P. Chen, J. Wang, L. Wang, Y. Xu, Perforated cenospheres: A reactive internal curing agent for alkali activated slag mortars, Cem. Concr. Compos. 104 (2019), https://doi.org/10.1016/j.cemconcomp.2019.103351.

[18] J. Zhang, Q. Wang, J. Zhang, Shrinkage of internal cured high strength engineered cementitious composite with pre-wetted sand-like zeolite, Constr. Build. Mater. 134 (2017) 664–672, https://doi.org/10.1016/j.conbuildmat.2016.12.182.

[19] C. Rößler D.-D. Bui H.-M. Ludwig Rice husk ash as both pozzolanic admixture and internal curing agent in ultra-high performance concrete Cem. Concr. Compos. 53 (2014) 270–278https://doi.org/10.1016/j.cemconcomp.2014.07.015.

[20] B. Mohr, L. Premenko, H. Nanko, K. Kurtis, Examination of wood-derived powders and fibers for internal curing of cement-based materials, in: Proceedings of the 4th interntational Seminar: Self-Desiccation and Its Importance in Concrete Technology, 2005, pp. 229–244.

[21] X. Ma J. Liu C. Shi A review on the use of LWA as an internal curing agent of high performance cement-based materials Constr. Build. Mater. 218 (2019) 385–393https://doi.org/10.1016/j.conbuildmat.2019.05.126.

[22] S. Zhutovsky, K. Kovler, A. Bentur, Revisiting the protected paste volume concept for internal curing of high-strength concretes, Cem. Concr. Res. 41(9) (2011) 981-986https://doi.org/10.1016/j.cemconres.2011.05.007.

[23] P. Schwesinger, Reducing Shrinkage in HPC by International Curing Using Pre Soaked LWA, Control of Cracking in Early Age Concrete (2002) 333–338.

[24] S. Papatzani, E.G. Badogiannis, K. Paine, The pozzolanic properties of inorganic and organomodified nano-montmorillonite dispersions Constr, Build. Mater. 167 (2018) 299–316, https://doi.org/10.1016/j.conbuildmat.2018.01.123.

[25] O. Heinz, H. Heinz, Cement Interfaces: Current Understanding, Challenges, and Opportunities, Langmuir 37(21) (2021) 6347-6356https://doi.org/10.1021/acs.langmuir.1c00617.

[26] R. Fernandez, F. Martirena, K.L. Scrivener, The origin of the pozzolanic activity of calcined clay minerals: A comparison between kaolinite, illite and montmorillonite, Cem. Concr. Res. 41 (1) (2011) 113–122, https://doi.org/10.1016/j.cemconres.2010.09.013.

[27] V.A. Baki, X. Ke, A. Heath, J. Calabria-Holley, C. Terzi, M. Sirin, The impact of mechanochemical activation on the physicochemical properties and pozzolanic reactivity of kaolinite, muscovite and montmorillonite, Cement and Concrete Research 162 (2022), https://doi.org/10.1016/j.cemconres.2022.106962.

[28] N. Garg, J. Skibsted, Thermal activation of a pure montmorillonite clay and its reactivity in cementitious systems, J. Physic. Chem. C. 118 (21) (2014) 11464–11477, https://doi.org/10.1021/jp502529d.

[29] T.-P. Chang, J.-Y. Shih, K.-M. Yang, T.-C. Hsiao, Material properties of Portland cement paste with nano-montmorillonite, J. Mater. Sci. 42 (17) (2007) 7478–7487, https://doi.org/10.1007/s10853-006-1462-0.

[30] S. Papatzani, Effect of nanosilica and montmorillonite nanoclay particles on cement hydration and microstructure, Mater. Sci. Technol. 32 (2) (2016) 138–153, https://doi.org/10.1179/1743284715Y.0000000067.

[31] J. Wei, B. Gencturk, A. Jain, M. Hanifehzadeh, Mitigating alkali-silica reaction induced concrete degradation through cement substitution by metakaolin and bentonite Appl, Clay Sci. 182 (2019), https://doi.org/10.1016/j.clay.2019.105257.

[32] N. Mesboua, K. Benyounes, A. Benmounah, Study of the impact of bentonite on the physico-mechanical and flow properties of cement grout, Cogent Eng. 5 (1) (2018), https://doi.org/10.1080/23311916.2018.1446252.

[33] S. Khandelwal, K.Y. Rhee, Effect of silane modified smectite clay on the hydration, intercalation of PCE superplasticizers, and mechanical strength of cement composites, Cem. Concr. Compos. 123 (2021), https://doi.org/10.1016/j.cemconcomp.2021.104210.

[34] D. Luo, J. Wei, Hydration kinetics and phase evolution of Portland cement composites containing sodium-montmorillonite functionalized with a Non-Ionic surfactant Constr, Build. Mater. 333 (2022), https://doi.org/10.1016/j.conbuildmat.2022.127386.

[35] J.-A. Oh, Y. Zhuge, S. Araby, R. Wang, H. Yu, W. Fan, M. Liu, S.-H. Lee, M.J. Alam, J. Ma, Cement nanocomposites containing montmorillonite nanosheets modified with surfactants of various chain lengths Cem, Concr. Compos. 116 (2021), https://doi.org/10.1016/j.cemconcomp.2020.103894.

[36] M.K. Moraes, E.M. da Costa, Effect of adding organo-modified montmorillonite nanoclay on the performance of oil-well cement paste in CO2-rich environments Cem, Concr. Compos. 127 (2022), https://doi.org/10.1016/j.cemconcomp.2021.104210.

[37] D. Luo, J. Wei, Upgrading sodium montmorillonite into a reactive internal curing agent for sustainable cement composites through non-ionic functionalization, Compos B Eng 242 (21) (2022), https://doi.org/10.1016/j.compositesb.2022.110076.

[38] ASTMC150/C150M, Standard Specification for Portland Cement, 2021.

[39] ASTMC837, Standard test method for methylene blue index of clay, ASTM, 2019.

[40] K. Taleb, I. Pillin, Y. Grohens, S. Saidi-Besbes, Gemini surfactant modified clays: Effect of surfactant loading and spacer length, Appl. Clay Sci. 161 (2018) 48–56, https://doi.org/10.1016/j.clay.2018.03.015.

[41] M.L. Whittaker, L.N. Lammers, S. Carrero, B. Gilbert, J.F. Banfield, Ion exchange selectivity in clay is controlled by nanoscale chemical–mechanical coupling, Proceedings of the National Academy of Sciences 116 (44) (2019) 22052–22057, https://doi.org/10.1073/pnas.1908086116.

[42] X. Pang, L. Sun, F. Sun, G. Zhang, S. Guo, Y. Bu, Cement hydration kinetics study in the temperature range from 15° C to 95° C Cem, Concr. Res. 148 (2021), https://doi.org/10.1016/j.cemconres.2021.106552.

[43] ASTMC1074, Standard practice for estimating concrete strength by the maturity method, 1074 (2017) https://doi.org/10.1520/C1074-17.

[44] T. Kim, J. Olek, Effects of sample preparation and interpretation of thermogravimetric curves on calcium hydroxide in hydrated pastes and mortars, Transp. Res. Rec. 2290 (1) (2012) 10–18, https://doi.org/10.3141/2290-02.

[45] J.I. Bhatty, Hydration versus strength in a portland cement developed from domestic mineral wastes—A comparative study, Thermochim. Acta 106 (1986) 93–103, https://doi.org/10.1016/0040-6031(86)85120-6.

[46] T.C. Powers, T.L. Brownyard, Studies of the physical properties of hardened Portland cement paste, J. Proc. (1946) 101–132.

[47] J. Tikkanen, A. Cwirzen, V. Penttala, Effects of mineral powders on hydration process and hydration products in normal strength concrete Constr, Build. Mater. 72 (2014) 7–14, https://doi.org/10.1016/j.conbuildmat.2014.08.066.

[48] S. Gražulis, D. Chateigner, R.T. Downs, A. Yokochi, M. Quirós, L. Lutterotti, E. Manakova, J. Butkus, P. Moeck, A. Le Bail, Crystallography Open Database–an open-access collection of crystal structures, J. Appl. Crystallogr. 42 (4) (2009) 726–729, https://doi.org/10.1107/S0021889809016690.

[49] ASTMC1608, Standard test method for chemical shrinkage of hydraulic cement paste, 2017.

[50] ASTMC109/C109M, Standard Test Method for Compressive Strength of Hydraulic Cement Mortars (Using 2-in. or [50-mm] Cube Specimens), 2020.

[51] Y. Sargam, K. Wang, Hydration kinetics and activation energy of cement pastes containing various nanoparticles, Compos B Eng 216 (2021), https://doi.org/10.1016/j.compositesb.2021.108836.

[52] J.W. Bullard, H.M. Jennings, R.A. Livingston, A. Nonat, G.W. Scherer, J. S. Schweitzer, K.L. Scrivener, J.J. Thomas, Mechanisms of Cement hydration, Cem. Concr. Res. 41 (12) (2011) 1208–1223, https://doi.org/10.1016/j.cemconres.2010.09.011.

[53] X. Pang, L. Sun, M. Chen, M. Xian, G. Cheng, Y. Liu, J. Qin, Influence of curing temperature on the hydration and strength development of Class G Portland cement Cem, Concr. Res. 156 (2022), https://doi.org/10.1016/j.cemconres.2022.106776.

[54] M. Boháč, R. Novotný, J. Tkacz, M. Hajdúchová, M. Palou, T. Staněk, The Role of Temperature on Hydration of Binary System of Metakaolin/Portland Cement, Trans Tech Publ, Mater. Sci. Forum, 2016, pp. 51–56.
[55] S. Bishnoi, K.L. Scrivener, Studying nucleation and growth kinetics of alite hydration using μic Cem, Concr. Res. 39 (10) (2009) 849–860, https://doi.org/10.1016/j.cemconres.2009.02.002.
[56] K.A. Riding, J. Poole, K.J. Folliard, M.C. Juenger, A.K. Schindler, New Model for Estimating Apparent Activation Energy of Cementitious Systems, ACI Mater. J. 108 (5) (2011), https://doi.org/10.14359/51683265.
[57] K.O. Kjellsen, R.J. Detwiler, Reaction kinetics of Portland cement mortars hydrated at different temperatures, Cem. Concr. Res. 22 (1) (1992) 112–120, https://doi.org/10.1016/0008-8846(92)90141-H.
[58] Q. Xu, J. Hu, J.M. Ruiz, K. Wang, Z. Ge, Isothermal calorimetry tests and modeling of cement hydration parameters, Thermochim. Acta 499 (1–2) (2010) 91–99, https://doi.org/10.1016/j.tca.2009.11.007.
[59] F. Han, Z. Zhang, D. Wang, P. Yan, Hydration kinetics of composite binder containing slag at different temperatures, J. Therm. Anal. Calorim. 121 (2) (2015) 815–827.
[60] M. Broda, E. Wirquin, B. Duthoit, Conception of an isothermal calorimeter for concrete—Determination of the apparent activation energy, Mater. Struct. 35 (7) (2002) 389–394, https://doi.org/10.1007/BF02483141.
[61] V. Tydlitát, T. Matas, R. Černý, Effect of w/c and temperature on the early-stage hydration heat development in Portland-limestone cement, Constr. Build. Mater. 50 (2014) 140–147, https://doi.org/10.1016/j.conbuildmat.2013.09.020.
[62] H.C. Pedrosa, O.M. Reales, V.D. Reis, M. das Dores Paiva, E.M.R. Fairbairn, Hydration of Portland cement accelerated by CSH seeds at different temperatures, Cem. Concr. Res. 129 (2020), https://doi.org/10.1016/j.cemconres.2020.105978.
[63] G. Quercia, H. Brouwers, A. Garnier, K. Luke, Influence of olivine nano-silica on hydration and performance of oil-well cement slurries, Materials & Design 96 (2016) 162–170, https://doi.org/10.1016/j.matdes.2016.02.001.
[64] T. Zhang, P. Gao, R. Luo, Y. Guo, J. Wei, Q. Yu, Measurement of chemical shrinkage of cement paste: Comparison study of ASTM C 1608 and an improved method, Constr. Build. Mater. 48 (2013) 662–669, https://doi.org/10.1016/j.conbuildmat.2013.07.086.
[65] E. Gallucci, K. Scrivener, Crystallisation of calcium hydroxide in early age model and ordinary cementitious systems, Cem. Concr. Res. 37 (4) (2007) 492–501, https://doi.org/10.1016/j.cemconres.2007.01.001.
[66] R. Ylmén, U. Jäglid, B.-M. Steenari, I. Panas, Early hydration and setting of Portland cement monitored by IR, SEM and Vicat techniques, Cem. Concr. Res. 39 (5) (2009) 433–439, https://doi.org/10.1016/j.cemconres.2009.01.017.
[67] A. Govin, A. Peschard, R. Guyonnet, Modification of cement hydration at early ages by natural and heated wood, Cem. Concr. Compos. 28 (1) (2006) 12–20, https://doi.org/10.1016/j.cemconcomp.2005.09.002.
[68] F. Li, J. Liu, An experimental investigation of hydration mechanism of cement with silicane, Constr. Build. Mater. 166 (2018) 684–693, https://doi.org/10.1016/j.conbuildmat.2018.01.164.
[69] H. El-Hassan, N. Ismail, S. Al Hinaii, A. Alshehhi, N. Al Ashkar, Effect of GGBS and curing temperature on microstructure characteristics of lightweight geopolymer concrete, MATEC Web of Conferences 120 (2017) 03004, https://doi.org/10.1051/matecconf/201712003004.
[70] E. Scholtzová, L. Kucková, J. Kožíšek, D. Tunega, Structural and spectroscopic characterization of ettringite mineral–combined DFT and experimental study, J. Mol. Struct. 1100 (2015) 215–224, https://doi.org/10.1016/j.molstruc.2015.06.075.
[71] M.U. Okoronkwo, F.P. Glasser, Strätlingite: compatibility with sulfate and carbonate cement phases, Mater. Struct. 49 (9) (2016) 3569–3577, https://doi.org/10.1617/s11527-015-0740-1.
[72] M. Montes, E. Pato, P.M. Carmona-Quiroga, M.T. Blanco-Varela, Can calcium aluminates activate ternesite hydration? Cem. Concr. Res. 103 (2018) 204–215, https://doi.org/10.1016/j.cemconres.2017.10.017.
[73] M. Trezza, A. Lavat, Analysis of the system 3CaO· Al2O3–CaSO4· 2H2O–CaCO3–H2O by FT-IR spectroscopy, Cem. Concr. Res. 31 (6) (2001) 869–872, https://doi.org/10.1016/S0008-8846(01)00502-6.
[74] S. Khandelwal, K.Y. Rhee, Evaluation of pozzolanic activity, heterogeneous nucleation, and microstructure of cement composites with modified bentonite clays, Constr. Build. Mater. 323 (2022), https://doi.org/10.1016/j.conbuildmat.2022.126617.
[75] M. Chi, R. Huang, Effect of montmorillonite as additive on the properties of cement-based composites, Science and Engineering of Composite Materials 19 (1) (2012) 45–54, https://doi.org/10.1515/secm-2011-0129.
[76] P. Yu, Z. Wang, P. Lai, P. Zhang, J. Wang, Evaluation of mechanic damping properties of montmorillonite/organo-modified montmorillonite-reinforced cement paste, Constr. Build. Mater. 203 (2019) 356–365, https://doi.org/10.1016/j.conbuildmat.2019.01.110.
[77] Y. Wang, J. Yang, D. Ouyang, Effect of graphene oxide on mechanical properties of cement mortar and its strengthening mechanism, Materials 12 (22) (2019), https://doi.org/10.3390/ma12223753.
[78] D.P. Bentz, P.E. Stutzman, Internal curing and microstructure of high performance mortars, ACI SP-256, Laboratory and Field Experiences, Internal Curing of High Performance Concretes, 2008, pp. 81–90.
[79] L. Barcelo, M. Moranville, B. Clavaud, Autogenous shrinkage of concrete: a balance between autogenous swelling and self-desiccation, Cem. Concr. Res. 35 (1) (2005) 177–183, https://doi.org/10.1016/j.cemconres.2004.05.050.
[80] Q. Jiang, K. Wan, Improving internal curing efficiency through adjusting ab-and desorption curve of superabsorbent polymer in cement pastes using sodium carbonate, Cem. Concr. Compos. 129 (2022), https://doi.org/10.1016/j.cemconcomp.2022.104467.
[81] Z. Zhang, B. Zhang, P. Yan, Comparative study of effect of raw and densified silica fume in the paste, mortar and concrete, Constr. Build. Mater. 105 (2016) 82–93, https://doi.org/10.1016/j.conbuildmat.2015.12.045.